



**IMAGE PROCESSING BASED WIRELESS LOOP  
SCANNING SYSTEM IN HOT ROLLING MILLS  
AND REAL-TIME SCADA MONITORING**

**2023  
MASTERS THESIS  
ELECTRICAL&ELECTRONICS ENGINEERING**

**Kamal Uddin AQA**

**Thesis Advisor  
Assist.Prof.Dr. Hüseyin ALTINKAYA**

**IMAGE PROCESSING BASED WIRELESS LOOP SCANNING SYSTEM IN  
HOT ROLLING MILLS AND REAL-TIME SCADA MONITORING**



**Kamal Uddin AQA**

**Thesis Advisor  
Assist.Prof.Dr. Hüseyin ALTINKAYA**

**T.C.  
Karabuk University  
Institute of Graduate Programs  
Department of Electrical&Electronics Engineering  
Prepared as  
Master's Thesis**

**KARABUK  
June 2023**

I certify that in my opinion the thesis submitted by Kamal Uddin AQA titled “IMAGE PROCESSING BASED WIRELESS LOOP SCANNING SYSTEM IN HOT ROLLING MILLS AND REAL-TIME SCADA MONITORING” is fully adequate in scope and in quality as a thesis for the degree of Master of Science.

Assist. Prof. Dr. Hüseyin ALTINKAYA .....  
Thesis Advisor, Department of Electrical&Electronics Engineering

This thesis is accepted by the examining committee with a unanimous vote in the Department of Electrical&Electronics Engineering as a Master of Science thesis.  
June 21, 2023

<u>Examining Committee Members (Institutions)</u>	<u>Signature</u>
Chairman : Prof. Dr. Ziyodulla YUSUPOV (KBU)	.....
Member : Assist. Prof. Dr. Hüseyin ALTINKAYA (KBU)	.....
Member : Assist. Prof. Dr. Erdal ŞEHİRLİ (KU)	.....

The degree of Master of Science by the thesis submitted is approved by the Administrative Board of the Institute of Graduate Programs, Karabuk University.

Prof. Dr. Müslüm KUZU .....  
Director of the Institute of Graduate Programs



*“I declare that all the information within this thesis has been gathered and presented in accordance with academic regulations and ethical principles and I have according to the requirements of these regulations and principles cited all those which do not originate in this work as well.”*

Kamal Uddin AQA

## **ABSTRACT**

**M. Sc. Thesis**

### **IMAGE PROCESSING BASED WIRELESS LOOP SCANNING SYSTEM IN HOT ROLLING MILLS AND REAL-TIME SCADA MONITORING**

**Kamal Uddin AQA**

**Karabük University**

**Institute of Graduate Programs**

**The Department of Electrical and Electronics Engineering**

**Thesis Advisor:**

**Assist. Prof. Dr. Hüseyin ALTINKAYA**

**June 2023, 81 pages**

In this study, a novel approach is presented for scanning the loops in hot rolling mills using an image processing-based wireless loop scanning system and real-time SCADA (Supervisory Control and Data Acquisition) analysis. The proposed system offers several advantages over traditional scanning methods, such as improved accuracy, real-time monitoring, and remote access. The proposed system captures images of the loops and processes them using advanced image processing algorithm to perform the loop scanning process efficiently. The analyzed data is then monitored in real-time using SCADA software and the looper system is thus controlled. The wireless nature of the system allows it to be installed in difficult-to-use areas, while its real-time monitoring capabilities enable prompt response to any abnormalities. The system offers an innovative and efficient solution for scanning loops in hot rolling mills as compared to the conventional loop scanning methods that use sensors. Our study can provide significant benefits to manufacturers, enabling them

to reduce waste caused by flaws in the sensor while detecting the loops. The results of image-processing-based loop scanner can be reliable, making it a significant advancement in hot rolling mill monitoring technology. The study has the potential to revolutionize the way loop scanners are implemented in rolling mills, providing a more accurate, reliable, and efficient way to control the position and shape of the strip. The use of STM32 microcontroller used for image processing opens up new possibilities for real-time monitoring and control of steel production processes, leading to improved quality and productivity.

**Key Words:** Loop Scanner, Image Processing, SCADA, STM32.

**Science Code:** 90521

## ÖZET

**Yüksek Lisans Tezi**

### **SICAK HADDEHANELERDE GÖRÜNTÜ İŞLEME TABANLI KABLOSUZ LOOP TARAMA SİSTEMİ VE GERÇEK ZAMANLI SCADA İZLEME**

**Kamal Uddin AQA**

**Karabük Üniversitesi**

**Lisansüstü Eğitim Enstitüsü**

**Elektrik Elektronik Mühendisliği**

**Tez Danışmanı:**

**Dr. Öğr. Üyesi Hüseyin ALTINKAYA**

**Haziran 2023, 81 sayfa**

Bu çalışmada, sıcak haddehanelerde oluşan loop'ları taramak için görüntü işleme tabanlı kablosuz loop tarama sistemi ve gerçek zamanlı SCADA (Denetleyici Kontrol ve Veri Toplama) analizi kullanılarak yeni bir yaklaşım sunulmaktadır. Önerilen sistem, geleneksel tarama yöntemlerine göre birçok avantaj sunmaktadır ve bu avantajlar arasında artırılmış doğruluk, gerçek zamanlı izleme ve uzaktan erişim yer almaktadır. Önerilen sistem, loop'un görüntülerini yakalar ve gelişmiş görüntü işleme algoritması kullanarak döngü tarama sürecini verimli bir şekilde gerçekleştirir. Analiz edilen veriler, gerçek zamanlı olarak SCADA yazılımı kullanılarak izlenir ve döngü sistemi bu şekilde kontrol edilir. Sistemin kablosuz yapısı, zor kullanım alanlarına kurulabilmesini sağlarken, gerçek zamanlı izleme özellikleri herhangi bir anormalliğe hızlı tepki verilmesini sağlar. Bu sistem, sensör kullanan geleneksel loop tarama yöntemlerine göre sıcak haddehanelerde loop'leri tarayan yenilikçi ve verimli bir çözüm sunmaktadır. Çalışmamız, üreticilere,

loop'leri algılamak sensördeki hatalardan kaynaklanan kayıpları azaltmalarına olanak tanıyarak önemli faydalar sağlayabilir. Görüntü işleme tabanlı loop tarayıcının sonuçları güvenilir olabilir, bu da sıcak haddeleme izleme teknolojisinde önemli bir ilerleme olarak değerlendirilebilir. Bu çalışma, loop tarayıcılarının haddehanelerde uygulanma şeklini devrim niteliğinde değiştirebilir ve çubuğun konumunu ve şeklini daha doğru, güvenilir ve verimli bir şekilde kontrol etmek için daha iyi bir yöntem sağlayabilir. Kullanılan STM32 mikrodenetleyici, çelik üretim süreçlerinin gerçek zamanlı izlenmesi ve kontrolü için yeni olanaklar sunarak kalite ve verimlilikte iyileşmeye yol açar.

**Anahtar Sözcükler :** Loop Tarayıcı, Görüntü İşleme, SCADA, STM32.

**Bilim Kodu:** 90521

## **ACKNOWLEDGEMENT**

I would like to express my deep and heartfelt gratitude to my supervisor Assist. Prof. Dr. Hüseyin ALTINKAYA, who supported me throughout this challenging as well as an incredible journey. The guidance, endless hours of assistance and encouragement provided by him have been invaluable. His dedication and expertise have shaped the success of this project.

I would also like to extend my gratitude to my family, especially my wife, for their unwavering encouragement, support and love. Without them, this perseverance and endeavor would not have been possible.

## TABLE OF CONTENTS

	<u>Page</u>
APPROVAL.....	ivi
ABSTRACT.....	iv
ÖZET.....	vi
ACKNOWLEDGEMENT .....	viii
TABLE OF CONTENTS.....	ix
LIST OF FIGURES .....	xii
SYMBOLS AND ABBREVIATIONS INDEX.....	xiv
CHAPTER 1 .....	1
INTRODUCTION .....	1
CHAPTER 2 .....	7
LITERATURE REVIEW.....	7
CHAPTER 3 .....	12
STEEL ROLLING MILLS .....	12
3.1. TYPES OF ROLLING PROCESS.....	12
3.1.1. Hot Rolling .....	13
3.1.2. Cold Rolling .....	14
3.2. FINISHED PRODUCTS .....	15
3.2.1. Hot Rolled Products .....	15
3.2.2. Cold Rolled Products .....	15
3.3. ROLLING MILL TYPES .....	16
3.3.1 Two High Rolling Mills.....	16
3.3.2 Three High Rolling Mills.....	16
3.3.3 Four High Rolling Mills .....	16
3.3.4 Cluster Mills .....	17
3.3.5 Tandem or Continuous Rolling Mills .....	17

	<u>Page</u>
3.4. LOOPER SYSTEM .....	17
3.4.1. Faulty Looper Operation .....	19
3.4.1.1. Low Tension between Stands .....	20
3.4.1.2. High Tension between Stands.....	20
3.5. CALCULATION OF STRIP TENSION .....	20
3.6. FEEDBACK SOURCES IN ROLLING MILLS .....	23
3.6.1. Hot Metal Detector (HMD) .....	23
3.6.2. Stand Threading Signal.....	23
3.6.3. Loop Scanner .....	23
CHAPTER 4 .....	26
MICROCONTROLLERS AND IMAGE PROCESSING.....	26
4.1. STM32F407G-DISC1 MICROCONTROLLER.....	26
4.1.1. Advanced Features of the STM32F407 .....	27
4.1.2. STM32 Peripherals .....	28
4.2. IMAGE PROCESSING BASED LOOP SCANNING .....	28
4.2.1. Advantages .....	28
4.2.2. Disadvantages .....	29
CHAPTER 5 .....	30
EXPERIMENTAL SETUP .....	30
5.1. LOOP SCANNER DESIGN .....	30
5.2. SCANNER'S ELECTRICAL COMPONENTS .....	33
5.2.1. ESP32 CAM .....	33
5.2.2. Voltage Regulator .....	33
5.2.3 STM32 Microcontroller.....	34
5.2.4 STM32 CubeMX .....	35
5.2.5 S7-1200 PLC .....	36
5.4. SOFTWARES AND PROGRAMMING .....	40
5.4.1 ESP32 CAM Programming .....	40
5.4.2 C# (C Sharp) Programming.....	41
5.4.3 STM32 Cube IDE Programming.....	49

	<u>Page</u>
5.4.4 TIA Portal Programming .....	51
CHAPTER 6 .....	56
CONCLUSIONS AND SUGGESTIONS.....	56
6.1. CONCLUSIONS .....	56
6.2. SUGGESTIONS.....	57
REFERENCES.....	59
APPENDIX A. ....	64
APPENDIX B. ....	68
APPENDIX C. ....	74
RESUME .....	81

## LIST OF FIGURES

	<u>Page</u>
Figure 1.1. World volume of steel related trade 2000 to 2021 [3].	1
Figure 1.2. 11-months finished product of EU exports by products – monthly average - tonnes (2022) [5].	2
Figure 1.3. 11-months finished product exports of EU by countries – monthly average - tonnes (2022) [5].	2
Figure 1.4. 11-Months finished product imports of EU by products – monthly average - tonnes (2022) [5].	3
Figure 1.5. 11-Months finished product imports of EU by countries – monthly average - tonnes (2022) [5].	4
Figure 3.1. Traditional hot rolling mill’s schematic diagram [40].	12
Figure 3.2. Grain refinement in hot rolling [41].	13
Figure 3.3. Cold rolling in mill.	14
Figure 3.4. Continuous rolling mill.	17
Figure 3.5. (a) and (b) looper system.	18
Figure 3.6. Looper angle (a) increased & (b) decreased.	19
Figure 3.7. Tension and looper control in rolling mills (Source: IEEE xplore)	24
Figure 3.8. Loop formation in hot rolling mill.	25
Figure 3.9. Harsh conditions of hot rolling mill.	25
Figure 4.1. STM32F407G-DISC1 microcontroller.	27
Figure 5.1. Loop scanner design.	31
Figure 5.2. Camera aperture on loop scanner.	31
Figure 5.3. Side view of loop scanner.	32
Figure 5.4. Inner view of loop scanner.	32
Figure 5.5. ESP32 cam module.	33
Figure 5.6. Voltage regulator circuit diagram.	34
Figure 5.7. Voltage regulator circuit.	34
Figure 5.8. STM32 CubeMX configuration.	35
Figure 5.9. STM32 CubeMX middleware config.	36
Figure 5.10. STM32 CubeMX clock configuration.	36

Figure 5.11. Simatic S7-1200 PLC. ....	37
Figure 5.12. 24V power supply. ....	38
Figure 5.13. Mechanical setup for loop scanning test. ....	38
Figure 5.14. Resistance wire used in mechanical setup. ....	39
Figure 5.15. Loop scanner detecting resistance wire. ....	39
Figure 5.16. Block diagram of loop scanning system. ....	40
Figure 5.17. Image processing flow chart. ....	47
Figure 5.18. Loop scanner application display I. ....	48
Figure 5.19. Loop scanner application display II. ....	48
Figure 5.20. Loop scanner application display II. ....	49
Figure 5.21. Device&Networks view. ....	51
Figure 5.22. Portal view. ....	51
Figure 5.23. Device config. view. ....	52
Figure 5.24. Ladder diagram of OUT_RANGE function. ....	52
Figure 5.25. Ladder diagram of NORM_X & SCALE_X. ....	53
Figure 5.26. Function block. ....	53
Figure 5.27. SCADA screen 1. ....	54
Figure 5.28. SCADA screen 2. ....	55
Figure 5.29. SCADA screen 3. ....	55
Figure 6.1. Defected traditional sensors. ....	57

## SYMBOLS AND ABBREVIATIONS INDEX

### SYMBOLS

$A$  : strip cross section

$\sigma$  : unit tension

$j$  : moment of inertia

$T_L$  : load torque

$T_R$  : cylinder torque

$\omega$  : looper angle

## ABBREVIATIONS

AC	:	Alternative Current
ADC	:	Analog to Digital Converter
AI	:	Analog Input
AO	:	Analog Output
C#	:	CSharp
CNNs	:	Convolutional Neural Networks
CPU	:	Central Processing Unit
DC	:	Direct Current
DI	:	Digital Input
DO	:	Digital Output
FPU	:	Floating Point Unit
GPIO	:	General Purpose Input Output Layer
GUI	:	Graphical User Interface
HAL	:	Hardware Abstraction Layer
HMD	:	Hot Metal Detector
IDE	:	Integrated Development Environment
LBP	:	Local Binary Pattern
LED	:	Light Emitting Diode
PLC	:	Programmable Logic Controller
PWM	:	Pulse Width Modulation
SCADA	:	Supervisory Control and Data Acquisition
SEM	:	Scanning Electron Microscope
STD	:	Stand
TIA	:	Totally Integrated Automation
UART	:	Universal Asynchronous Receiver Transmitter
YOLO	:	You Only Look Once
3D	:	3-Dimensional

## **CHAPTER 1**

### **INTRODUCTION**

For decades, rolling mills have played an essential role in the advancement of the steel industry. The steel production industry is a significant contributor to global economic development having a wide range of applications in manufacturing, construction and transportation. The steel industries produce hot rolled steel and the finished product has important applications in large sectors such as automotive [1], appliance manufacturing, bridges [2], electric motors etc. which have great use in industrial as well as daily use products. The rolling process requires precise control during the production of high-quality steel products in order to ensure efficient use of resources and consistent product quality.

The production of steel is an essential factor in various industries, playing a crucial role in the creation of infrastructure, consumer goods, and automobiles. This adaptable alloy, which consists mainly of carbon and iron, is a key material in the development of modern civilization. With the world's population and urbanization continually increasing, the demand for steel products continues to grow, leading to an expansion in the global steel industry. As a result, steel production has become a significant contributor to economic growth worldwide, with nations striving to enhance their production capabilities to meet the escalating demand. Figure 1.1 shows the volume of steel manufactured goods, steel and all other commodities in million tons starting from the year 2000 to 2020 [3]. The volume of steel production and steel related products are observed to be at surprising rate with an upwards trend in 2020.



Figure 1.1. World volume of steel related trade 2000 to 2021 [3].

Despite an increased demand, there was a significant decline in global steel production in 2022, with a 4.2% decrease compared to the previous year, resulting in a total production of 1.8 billion tons. Similarly, Turkey experienced a notable reduction of 12.9% in steel production in 2022, with a total output of 35.1 million tons. According to the World Steel Association, Turkey dropped from seventh to eighth place in global crude steel production in 2022, with a 12.9% decrease to 35.1 million tons [4]. Germany also experienced an 8.4% decrease to 36.8 million tons. Meanwhile, China maintained its lead with 1.013 billion tons, followed by India at 124.7 million tons, and Japan at 89.2 million tons. The United States remained in fourth place with 80.7 million tons, while Russia and South Korea followed in fifth and sixth place, respectively.

According to reports, in the first eight months of 2022, the exports of all flat products were found to be decreased, with a 26% decrease in organic coated sheet exports, a 23% decrease in hot-dip galvanized sheet exports, and a 12% decrease in cold-rolled sheet exports. However, there was a 7% increase in hot-rolled strip exports and a 2% increase in quarto sheet exports. Among long products, a decrease of 24% in commercial bar exports, 23% in construction steel exports, and 20% in heavy profile and film-laminated steel exports was reported [5].

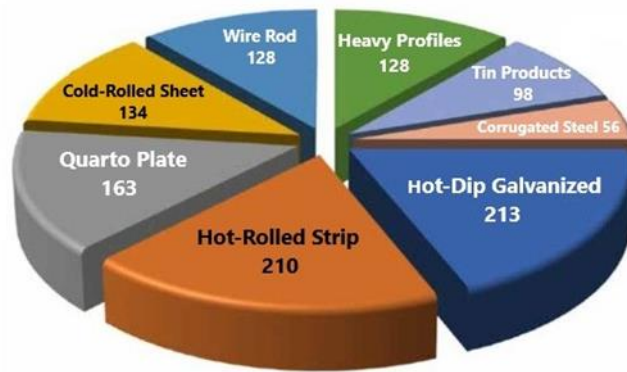


Figure 1.2. 11-months finished product of EU exports by products – monthly average - tonnes (2022) [5].

In the initial eight months of 2022, Turkey, the UK, the US, Switzerland, and China were highlighted as the most crucial markets for the EU steel product exports, followed by Norway, Egypt, Brazil, and India, which collectively accounted for 58% of the total finished product exports. It was reported that while exports to Brazil increased by 47%, exports to the United States increased by 9%, and exports to Norway increased by 5% in the same period, exports to other key markets declined. The most significant decreases in the EU export goals were observed in Russia, with a 63% decline, followed by a 34% decrease in exports to China, a 22% drop in exports to the United Kingdom, a 9% reduction in exports to Turkey, an 8% decline in exports to India, a 4% decrease in exports to Egypt, and a 1% reduction in exports to Switzerland.

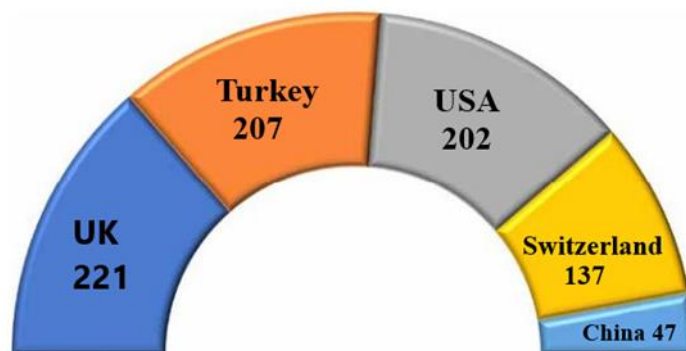


Figure 1.3. 11-months finished product exports of EU by countries – monthly average - tonnes (2022) [5].

The data from customs reveal that during the first eight months of 2022, there was an increase of 6% in the import of flat products and 16% in the import of long products in EU. It's worth noting that the share of long products in the overall import of finished steel products was 23%. In the second quarter of 2022, the import of flat products went down by 1%, whereas the import of long products increased by 14%, leading to an overall 2% increase in the import of finished products.

As for the flat products, the import of majority of the products was found to be increased during the first eight months of 2022 as compared to the same period in 2021. Coated sheets had the highest increase with a 43% rise, while cold-rolled sheet imports increased by 23%, and hot-dipped imports increased by 5%. On the other hand, imports of hot-rolled strip decreased by 6%, and imports of quarto plate decreased by 10%, respectively.

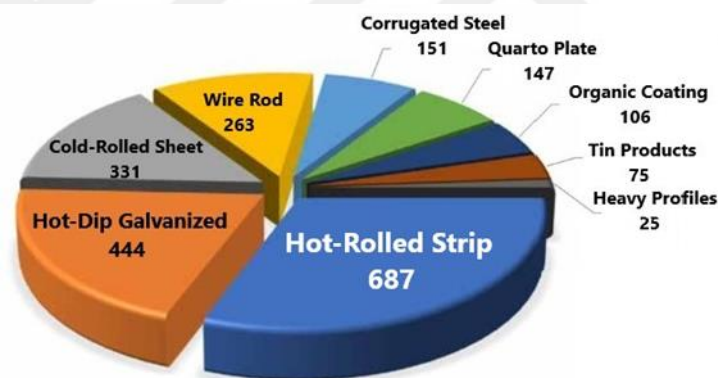


Figure 1.4. 11-Months finished product imports of EU by products – monthly average - tonnes (2022) [5].

According to reports, Turkey, India, South Korea, China, and Taiwan were the primary countries from which the EU market imported final products during the first eight months of 2022, while Russia and Ukraine experienced significant decreases in imports due to EU sanctions and the negative effects of the war. Notably, neither country ranked among the top five countries that the EU imports from. The top five countries, which collectively account for 51% of total EU final product imports, are Turkey (15.4%), India (10.6%), South Korea (9.5%), China (8.5%), and Taiwan (6.9%). Third-country final product imports increased by 8% during the first eight

months of 2022, with China experiencing a 109% increase, followed by South Korea (42%), Taiwan (41%), and Turkey (7%), while India saw a 6% decrease in imports.

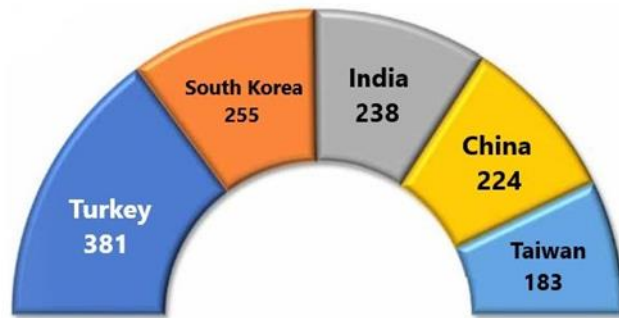


Figure 1.5. 11-Months finished product imports of EU by countries – monthly average - tonnes (2022) [5].

As the process performed in steel mills is a complicated process and requires precise control, determining the position of the strip being rolled is an important task, and in order to achieve these objectives, ‘Loop scanners’ have emerged as an essential device, providing real-time feedback on the position of the strip and enabling the production of high-quality metal products with reduced energy consumption and improved sustainability.

There has been an increasing demand for loop scanners recently. The use of loop scanners has become increasingly common in steel industries due to their potential to improve the efficiency and performance. Loop scanners provide reliable and accurate detection of the strip position, thus allowing for better control conducted by the looper system installed in the rolling mill. The data provided by loop scanners can be used to adjust the tension of the loop in the rolling process. The tension needs to be kept at appropriate range and max. – min.- threshold ought to be considered in determined intervals. Adjusting the tension precisely yields improved quality and lower production wastes. The working principle, type and application of loop scanners are well-known. However, there is still a research gap regarding their impact on the performance of rolling mills. Traditional loop scanners use sensors to detect the strip position, which can be expensive, unreliable and prone to errors. The use of image-processing in loop scanners can be a promising solution for the problems encountered in traditional loop scanners.

The steel strip rolling is a sequential process which is carried out to convert the slab in a semi-finished form to a finished hot coil formed strip. The slab obtained after different processes is reheated to a fixed temperature and then rolled to make the hot strip in a coiled form. The rolling mill consists of the following areas: Furnace Area, Roughing mill, Intermediate mill and Finishing mill. The slabs having 250-mm thickness are heated to approximately 1200°C temperature in the furnace area. In roughing mill, these slabs are rolled to 25–50 mm thickness. After undergoing different processes in the intermediate mill, the resulting slab is passed to the finishing mill. In the finishing mill, the product is further reduced to a final thickness of approximately 0.8–20 mm.

In recent years, image processing techniques and microcontroller technology have developed rapidly, opening up possibilities and providing new ways for designing loop scanners using cameras and microcontrollers. The use of microcontrollers and cameras can provide a more efficient, accurate and reliable way to detect the position of the strip. Determining the position of the strip changing at rapid rate has been challenging since the initial days of the invention of the looper system. By providing data collected through camera and microcontroller, loop scanners can play a crucial role in addressing the afore-mentioned challenges.

Rolling mills are supposed to maintain high levels of productivity without compromising on stringent quality standards to meet current market demands. The control system in the rolling process plays a vital role in ensuring the correct operation of each link in the equipment chain, thus achieving high and sustainable production rates. In this case, productivity is influenced by various factors such as automation levels, facility layout, equipment condition, pass design, operator training and maintenance. It can be measured in various ways, such as output per unit of input. In order to be considered a commercial product, the steel produced needs to comply with the quality standards of steel grade. In short, productivity represents the efficiency of production.

The literature review of different studies that have used image processing in the steel rolling mills is presented in Chapter 2. Background information related to Steel

Rolling Mills as well as Looper system is given in Chapter 3. STM32 Microcontroller is explained briefly in Chapter 4. The prototype design and information regarding the hardware and software used in the design is given in Chapter 5. The key findings and conclusions of the thesis are presented in the final chapter, Chapter 6.



## CHAPTER 2

### LITERATURE REVIEW

In steel production industries, the use of image processing technologies has become increasingly popular in recent years. The image processing technologies along with microcontrollers offer different benefits including increased product quality, improved accuracy and efficiency in production processes, and most importantly reduced costs. Image processing can be particularly useful in loop scanning, a process used to monitor and control the shape and position of the metal strip as it passes through the rolling mill.

With the advancement of image processing algorithms and imaging systems, a new field of instrumentation and quality control has emerged, and the advances observed in this field have been presented recently [6].

Several algorithms used for optimization of threshold values have been reported in the literature. In a study conducted by Hongnan et al., modified grasshopper optimization algorithm was used for thresholding the color image segmentation [7]. In a similar study, Zhang et al. proposed the novel bee foraging algorithm that was based on a multilevel thresholding value used for colored image segmentation [8].

The image processing is currently being used for inspection systems that detect abnormalities on metal surfaces before the packaging process. Such inspection systems are being considered in different applications and the achieved results are found to be promising [9–11]. The inspection systems use detection devices which include industrial cameras, protection devices and light sources, etc.

In different studies, researchers have conducted significant studies on the detection of defects found on steel strip surfaces using machine learning algorithms. In their

study on classification of steel, Karthikeyan et al. reported that the magnification of defects provides a solution to analyse the defects on steel surfaces at micro level in SEM images [12]. Overall accuracy of up-to 96.7% was obtained which determines that the proposed method has a better accuracy as compared to previous methods.

A similar study by Zaghoudi et al. implemented the k-nearest neighbor algorithm to detect defects on steel strip [13]. According to the experimental results, the method was found to be efficient and simple. Furthermore, the steel inspection system in their study provided better results and an accuracy of 93.33%.

Samsudin et al. presented a technique that utilizes the local binary pattern to categorize images based on six distinct defect classes observed on rolled steel surfaces [14]. Zhang et al. introduced a novel fuzzy defect detection method for sets that differed from conventional methods by incorporating a membership function to determine if a given grey level could potentially indicate a defect. When implemented with pixel connectivity, this method could accurately identify defects with a high degree of accuracy [15].

In a study conducted by Liu et al., the LBP algorithm was applied to recognize the defects found on steel strip surface [16]. Although machine learning approaches can achieve promising results, they have certain limitations that need to be considered. Firstly, traditional machine learning methods require feature extraction, which can constrain the algorithms' effectiveness. Additionally, the accuracy of machine learning classification is often insufficient. Therefore, deep learning technology has become increasingly prevalent in the identification and classification of steel strip surface defects due to its significant progress in recent years.

Liu et al. conducted a study that led to the development of a new classification model that is found to be effective in identifying defects on steel plate surfaces [17]. Experimental results demonstrate that this model offers several advantages, including high speed and accurate classification, especially when working with corrupted datasets.

Li et al. constructed a dataset that includes six distinct types of surface defects found in cold-rolled steel [18]. To mitigate over-fitting, they augmented the dataset. They also enhanced the You Only Look Once (YOLO) network and converted it into a convolutional model. The resulting network, comprising 27 convolution layers, provides a comprehensive approach for identifying defects on steel-strip surfaces. When applied to the six defect types, their network demonstrated an impressive 97.55% performance and a recall rate of 95.86%, respectively.

Recent research has shown considerable interest in combining convolutional neural networks (CNNs) with self-attention mechanisms, either by enhancing feature maps for image classification [19] or by processing CNN outputs using self-attention for tasks such as object detection [20-21], video processing [22], image classification [23], and unsupervised object discovery [24].

Additionally, image GPT (iGPT) [25] is a recent model that employs transformers on low-resolution, and low-color images in an unsupervised generative fashion. The resulting representation can be fine-tuned or probed linearly for classification performance, with a maximum accuracy of 72% on ImageNet.

Wang et al. devised an online approach to detect 3D defects utilizing photometric stereo, allowing for precise localization and identification of sheet steel defects [26]. To enable online detection of high-speed steel, a photometric laser scanning system was developed. This system effectively mitigated the impact of "pseudo-defect" disturbances, thus resulting in significantly improved detection accuracy.

In a study performed by Xie et al., incorporating additional data sources was found to yield state-of-the-art results on conventional benchmarks [27]. Furthermore, Sun et al. examined the correlation between dataset size and CNN performance [28], while Kolesnikov et al. [29] and Djolonga et al. [30] conducted an empirical research on CNN transfer learning using large-scale datasets such as JFT-300M and ImageNet-21k.

In a study conducted by Xue et al., the defects on samples were identified using various edge detection approaches and thin edge features were obtained on those samples [31]. Additionally, researchers have explored several machine learning techniques for classifying surface defects on rolled steel [32].

In a novel research by Zhao et al., a CNN model was introduced to extract small-scale bolt features with 71.4% accuracy [33]. Another study by Liu et al. used a CNN architecture to detect catenary support components (CSCs) by integrating a detection network for CSCs with a cascade network for detecting small-scale CSCs using Faster R-CNN. This model achieved a high accuracy of 92.8% [34].

In a study, Song et al. introduced a technique based on CNN for detecting defective screws, including damaged screws, surface dirt, and stripped screws. They captured images using an industrial camera and achieved 98% accuracy with an average processing time of 1.2 seconds per image [35].

Taheritanjani et al. developed a system for detecting damage in fasteners and identifying their type using machine learning models. The supervised model achieved 99% accuracy, while the unsupervised model achieved 84% accuracy [36].

Due to the high temperatures involved, measuring the speed of a billet as it moves along a rolling mill is a challenging task as the product is malleable and does not behave like a solid material. The range of speeds at which the product moves is vast, with speeds ranging from 0.5 meters per second at the beginning of the rolling mill to about 100 m/second at the end. To address this issue, Urbano et al. presented current sensors in their study that rely on laser technologies utilizing the Doppler effect [37]. In another study by Indu et al. detecting texture reliably was found to be crucial for accurately determining billet speed using optical flow techniques [38].

Souto et al. reported that various configuration parameters were employed during the image acquisition process and tests, depending on the specific stand, to obtain high-quality images. These parameters included resolution, with values ranging from 2048x1088 to 1056x600; frame rate, with values ranging from 73 to 153 frames per

second, and exposure time, with values ranging from 2500 to 2000 microseconds. According to their study, the utilization of cameras offered notable benefits over industrial devices, including greater flexibility, increased process data and information, and lower expenses [39].

This study tends to be a novel research on loop scanning using image processing as there were no studies found in the literature. There appears to be limited research specifically on image processing in rolling mills using CSharp and STM32. The studies mentioned above demonstrate the potential of image processing technologies for quality control in steel manufacturing. In particular, these studies suggest that image processing can be an effective tool for detecting defects in metal strips, which can lead to improved product quality and increased efficiency in the manufacturing process.

In conclusion, the literature suggests that image processing technologies have the potential to revolutionize quality control in steel manufacturing. While there is a need for further research specifically on image processing based loop scanning in rolling mills using CSharp and STM32, the existing literature provides valuable insights into the potential benefits and challenges of using image processing technologies in steel manufacturing.

## CHAPTER 3

### STEEL ROLLING MILLS

Rolling is a technique used in metal-working to decrease the thickness and create a consistent thickness throughout metal stock by passing it through one or more pairs of rolls. This method is similar to rolling dough. The temperature of the metal being rolled determines the classification of the process. The process of hot rolling steel strips involves several stages that aim to convert semi-finished slabs into hot strips in a coiled form. This process typically involves a reheat furnace, roughing mill, transfer table, coil box, crop shear, finishing mill, runout table, and coiler, as shown in Figure 3.1 below.

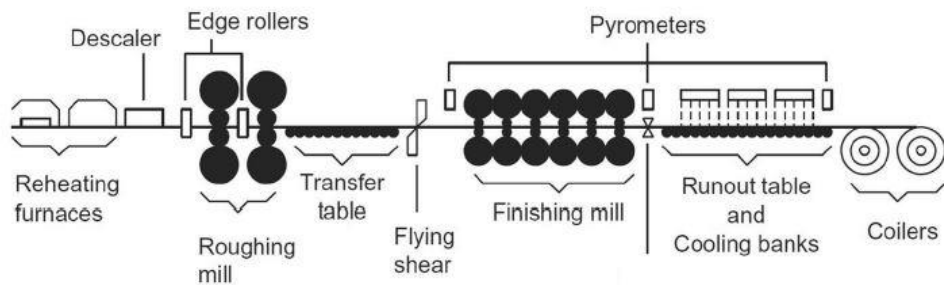


Figure 3.1. Traditional hot rolling mill's schematic diagram [40].

#### 3.1. TYPES OF ROLLING PROCESS

The main goal of the process is to reduce the thickness of the metal while increasing its length and keeping the width fluctuation to a minimum. The temperature in the rolling mill plays a significant role. If it is above its recrystallization point, the process is referred to as 'hot rolling', whereas, if the temperature is below the recrystallization point, it is referred to as cold rolling. The two types of rolling processes based on temperature are classified as follows:

### 3.1.1. Hot Rolling

For most steel products, the initial hot working operation is conducted on the primary roughing mill, which can be blooming, slabbing, or cogging mills. These mills usually consist of two high reversing mills with rolls of 0.6 to 1.4 meters in diameter, which are designated by their size. The process involves heating the steel above its recrystallization temperature and then deforming it between rollers. Hot rolling simplifies shaping and forming processes, and it is typically a faster and more cost-effective manufacturing method. The rolling process shown in Fig. 3 below converts the coarse structure of a cast ingot into a fine-grained structure. The hot rolling process is widely used in the manufacturing of various useful products, including rails, sheets, structural sections, plates, and more.

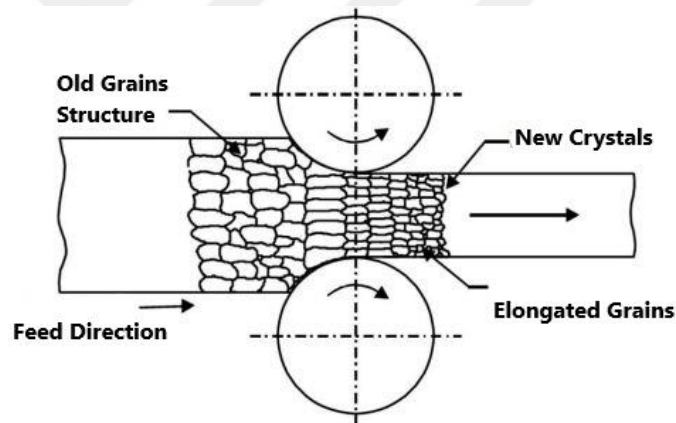


Figure 3.2. Grain refinement in hot rolling [41].

The aim of the hot rolling process is to break down the cast ingot into blooms or slabs that can be further processed into bars, plates, or sheets. To achieve this, the slabs are initially heated to a temperature of 1100-1300°C. In the finishing mill, the temperature should be maintained between 700-900°C, which is above the upper critical temperature. This ensures the production of uniform and equally sized product.

- To reduce the thickness of a flat plate with a large thickness of 10-50mm, it is passed through a series of working rolls that gradually decrease its thickness with each pass.

- The resulting hot strip is coiled to manage its increasing length caused by the reduction in thickness. This process helps to simplify the control of strips moving at different speeds due to varying thicknesses, as thinner sections tend to move faster.

### 3.1.2. Cold Rolling

Cold rolling is a metal forming process that involves reducing the thickness of a metal sheet under the recrystallization temperature. The starting material for cold rolled steel sheet is a pickled hot rolled breakdown coil obtained from the continuous hot rolling mill. The total reduction achieved by cold rolling typically ranges from 50 to 90%. To ensure uniform reduction in each pass, the reduction percentage should not fall below the minimum requirement.

The final pass generally has the lowest percentage reduction to allow for better control of flatness and surface finish. Cold rolling can produce products with good surface finish due to the absence of oxide scales caused by low temperature. Additionally, dimensional tolerance is improved as compared to hot rolled products due to less thermal expansion. Cold rolled sheet may be produced from hot rolled strip.

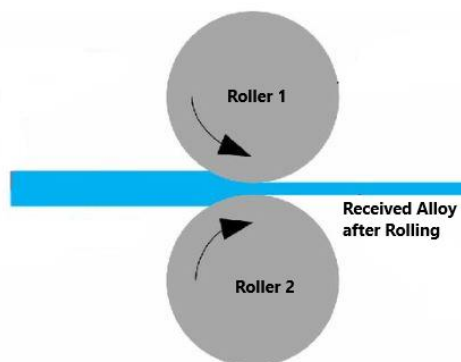


Figure 3.3. Cold rolling in mill.

## **3.2. FINISHED PRODUCTS**

The main finished products obtained after hot and cold rolling can be classified as follows:

### **3.2.1. Hot Rolled Products**

Hot rolled products are known to be obtained by the primary method for breaking down ingots into billets and blooms (obtained after the initial breakdown of an ingot, with a cross-sectional area greater than  $230 \text{ cm}^2$ ). This is typically followed by additional hot rolling to create a variety of products such as plates, rods, bars, pipes, rails, and more.

- A plate is a flat metal product with a thickness greater than 6 mm.
- A rod is a metal product with a cylindrical shape and a circular cross-section that is usually made through hot rolling.
- A bar, on the other hand, is a metal product that has a rectangular or square shape.

### **3.2.2. Cold Rolled Products**

Cold rolled products are obtained by the cold rolling process that has played an essential role in the steel industry. The process produces strips, sheets and foils with extra-ordinary surface finishes, increased mechanical strength, and precise control of product dimensions.

- A strip is a flat metal product with a thickness less than 6 mm and a width less than 600 mm.
- A sheet is a flat metal product with a thickness less than 6 mm and a width greater than 600 mm.
- A foil is a thin sheet of metal with a thickness less than 0.2 millimeters.

### **3.3. ROLLING MILL TYPES**

The rolling mills typically include three types of mills: roughing, intermediate, and finishing. The slabs, which are initially around 250-mm thick, are reheated to a temperature of about 1200°C in the reheat furnace before being reduced to a thickness of 25-50 mm in the roughing mill. The transfer bar is then sent to the finishing mill, where it is further reduced to a final thickness of 0.8-20 mm. The types of hot rolling mills that conduct the whole process of steel rolling are described briefly in this section.

#### **3.3.1 Two High Rolling Mills**

This mill comprises of two horizontal rolls rotating at an identical speed but in opposite directions. They're placed on bearings that are enclosed within robust upright side frames known as stands. The gap between the rolls can be changed by elevating or lowering the top roll. Additionally, in this type of mill, the material can be passed back and forth through the rolls by changing their direction of rotation.

#### **3.3.2 Three High Rolling Mills**

A three-high rolling mill is composed of three parallel rolls stacked vertically with the upper and lower rolls rotating in the same direction while the middle roll rotates in the opposite direction to the other two. This type of rolling mill is composed of three rolls, with one positioned above the other two. The upper and lower rolls rotate in the same direction, while the middle roll rotates in the opposite direction through friction with the material being rolled.

#### **3.3.3 Four High Rolling Mills**

This rolling mill can be considered as a variation of the two-high rolling mill but with smaller rolls. Typically, it has four horizontal rolls, with the middle two rolls having smaller sizes compared to the top and bottom rolls. The smaller diameter rolls are supported by larger diameter backup rolls as they have less strength and rigidity.

### 3.3.4 Cluster Mills

The cluster mill is a unique variant of the four-high rolling mill, specifically designed for rolling thin and hard materials. In this type of mill, each of the two smaller working rolls is supported by two or more of the larger backup rolls.

### 3.3.5 Tandem or Continuous Rolling Mills

A continuous rolling mill, also known as a tandem rolling mill, is comprised of multiple non-reversing two-high rolling mills placed in a sequence, allowing the material to pass through each one in turn. This configuration is ideal for large-scale production, as it can quickly produce a high volume of products. However, it may not be suitable for smaller quantities, as frequent setup changes may require significant time and labor.

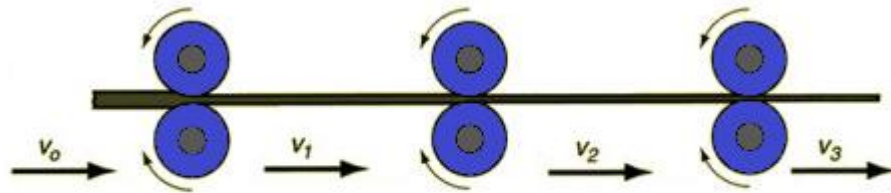


Figure 3.4. Continuous rolling mill.

## 3.4. LOOPER SYSTEM

Each mill in the rolling mill contains multiple Stands (STD), which are driven by individual AC or DC electric motors that are powered by either AC or DC drives, respectively. In order to ensure a consistent and high-quality rolling process, it is crucial to regulate the speed of the stands based on tension control and the speed ratios need to be kept constant between the stands. Any changes in the gap between the rolls can result in a potential increase or decrease in inter-stand tension. The tension between stands plays a significant role in determining the properties of the

workpiece produced in the mill. Therefore, it is necessary to monitor and adjust the rolling process to maintain appropriate tension levels and promptly identify and correct any deviations, enabling the production of high-quality workpieces that meet the desired specifications and standards.

The process occurs continuously, with wire rod passing through roll stands. This highlights the importance of a loop scanning system within the rolling mill. The looper system is responsible for managing tension control. Moreover, it plays a vital role in providing precise information regarding the head and tail end positions of the wire rod within the rolling mill. By accurately tracking the material, the system helps to ensure that the tension is controlled correctly, and the issues are identified and addressed quickly, thus enabling the smooth and efficient operation of the rolling mill.

Accurate material tracking is not only important for managing tension control, but it is also a fundamental requirement for various other aspects of the operation including automatic control sequences and data collection systems. Figure 3.5 (a) and (b) given below show the ‘Looper System’.

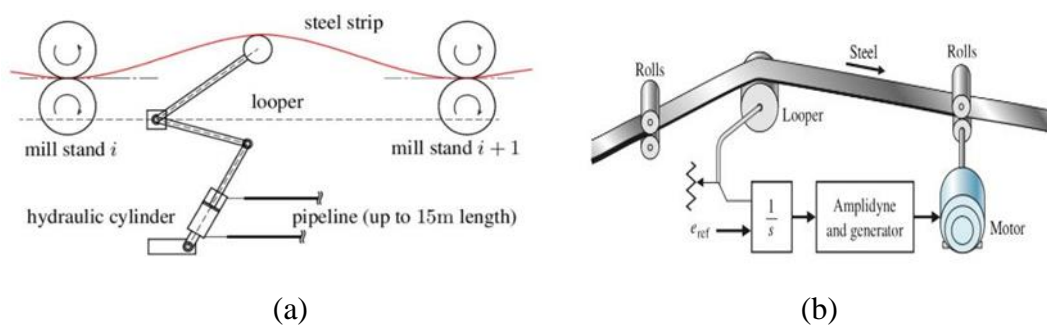


Figure 3.5. (a) and (b) looper system.

When strip tension is low between the finishing mill roll stands, the looper angle needs to be increased to increase strip tension, as illustrated in Figure 3.6. Whereas, when tension is high between the finishing mill roll stands, the looper angle should be decreased, as illustrated in Figure 3.7, in order to reduce the strip tension [42].

As the changes in strip height and length between roll stands affect the looper angle and torque, a flexible system is required to maintain a constant looper angle value and accommodate mass flow anomalies. Achieving precise control over looper angle and torque is crucial for ensuring high-quality output and efficient operations in finishing mills. However, maintaining this level of control can be difficult due to factors like uncertainty in parameters and non-linear system disturbances, which make looper angle and torque control challenging.

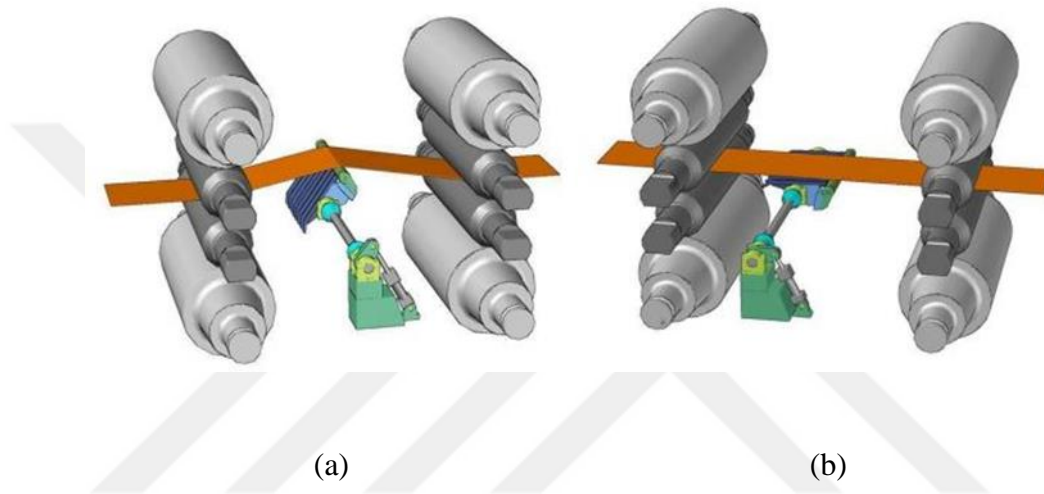


Figure 3.6. Looper angle (a) increased & (b) decreased.

### 3.4.1. Faulty Looper Operation

When the mass flow of the strip milled between the roll stands of the finishing mill is imbalanced, incorrect looper operation can cause fluctuations in strip tension, leading to quality defects and production impacts. There are four main reasons for mass flow imbalances, and if the finishing mill operator is unable to stabilize the system, it can have significant consequences. It is crucial to ensure proper looper operation to maintain stable strip tension and prevent quality defects. However, this can be a challenging task due to the non-linear nature of system disturbances and parameter uncertainties. Therefore, achieving accurate looper angle and torque control is a critical factor for successful finishing mill operations and ensuring high-quality strip production.

There are five primary defects that can arise in milled strips, including strip width reduction, rupture, bending, stretching, and dimensional variation [43]. These defects can occur due to incorrect looper operation and are typically caused by two main factors as follows:

#### **3.4.1.1. Low Tension between Stands**

Low tension between roll stands can cause an increase in the looper angle and strip height, leading to bending and further milling of bent strips. This situation may result in process interruption and even cylinder neck breakage.

#### **3.4.1.2. High Tension between Stands**

High tension between roll stands can reduce the looper angle and strip height, leading to material stretching and strip rupture between roll stands. In some cases, this requires changing either the work or rest milling cylinders due to incrustations or surface defects.

### **3.5. CALCULATION OF STRIP TENSION**

To determine the strip tension, the force exerted on the looper cylinder can be measured using pressure transducers installed in the cylinder piston and stem side cavities. This information is then used to calculate the tension and adjust the looper angle accordingly. Additionally, the tension calculated by the pressure load cell can serve as a backup or be used for viewing purposes.

Equation (1) provides a description of various components that contribute to the calculation of the looper load torque. The equation takes into account the looper moment of inertia, cylinder inertia, looper angular speed, and torque caused by the cylinder force. The looper load torque is the combined value of four torque components.

$$T_L = T_R - J \frac{d\omega}{dt} \quad (1)$$

$$T_R = T_{LP} = I_2 \cdot F_L \cos\left(\frac{\pi}{2} - \gamma - \psi\right) \quad (2)$$

Where; looper load torque is denoted by  $T_L$ , torque by cylinder is denoted as  $T_R$ , moment of inertia is given as  $J$  and looper angle is denoted by  $\omega$ .

The looper load torque, which is described by equation (1), is a combination of four torque components that work together to generate the total torque. These components are essential to understanding the behavior of the looper system and how it affects the overall process. The equation (3) and equation (4) are the formulations for torque caused by strip tension.

$$f_1 = (\theta)A\sigma \quad (3)$$

$$f_1(\theta) = R_1\{\text{sen}(\theta + \beta) - \text{sen}(\theta - \alpha)\} \quad (4)$$

Where; strip cross section is denoted by  $A$  and unit tension is denoted by  $\sigma$ . Strip weight's torque is formulated by equation (5).

$$f_2(\theta) = gR_1 \frac{W_s}{2} \cos \theta \quad (5)$$

The torque exerted by Looper weight is formulated in equation (6) as follows;

$$f_3(\theta)$$

$$f_3(\theta) = gR_G W_L \cos \theta \quad (6)$$

Equation (7) below formulates the torque of strip bending.

$$f_4(\theta)$$

$$f_4(\theta) = \frac{4E}{L^3} wh^3 (R_1 \sin \theta - H_1 - R_2) R_1 \cos \theta \quad (7)$$

From the equations,  $\alpha$ ,  $\beta$ ,  $W_S$  and  $T_L$  are calculated to be as follows:

$$\alpha = \tan^{-1} \frac{R_1 \sin \theta - H_1 - R_2}{L_1 + R_1 \cos \theta} \text{ (rad)} \quad (8)$$

$$\beta = \tan^{-1} \frac{R_1 \sin \theta - H_1 - R_2}{L - L_1 + R_1 \cos \theta} \text{ (rad)} \quad (9)$$

$$W_S = \rho WhL \cdot 10^{-9} \text{ (Kg)} \quad (10)$$

$$T_L = f_1 A \sigma + f_2(\theta) + f_3(\theta) + f_4(\theta) \quad (11)$$

The formulation thus derived for the tension is given in equation (12) below [44];

$$\sigma = \frac{T_L - (f_2(\theta) + f_3(\theta) + f_4(\theta))}{f_1(\theta) A} \text{ (Mpa)} \quad (12)$$

### **3.6. FEEDBACK SOURCES IN ROLLING MILLS**

There are typically three primary sources of feedback signals utilized in wire rolling mills [45-46], including:

#### **3.6.1. Hot Metal Detector (HMD)**

This is the most widely used sensor in mill lines, which relies on the detection of infra-red radiation emitted by hot materials. An optical system within the sensor receives the radiation, allowing the HMD to accurately detect the position of the material.

#### **3.6.2. Stand Threading Signal**

The stand threading signal is generated from either the peak torque detector in the drive or the PLC unit. This signal is crucial in the operation of the wire rod mill, providing valuable information regarding the position and movement of the material being processed.

#### **3.6.3. Loop Scanner**

This sensor is utilized in automatic loop control and works by optically scanning the field to be controlled. No optical adjustments are required for the loop scanners to function accurately.

In order to maintain a constant speed between the intermediate - roughing mill, and intermediate - finishing mill, a loop scanner is positioned between them. The loop scanner helps to ensure a smooth and consistent flow of material between the stands by sending analog signals to PLC for the adjustment of loop tension through looper system, thereby improving the overall quality and efficiency of the rolling process.

The looper system as shown in Figure 3.7 consists of a minute roller that is mounted on a pivoted arm and positioned below the mill pass line. When the head of the wire

rod enters the finishing mill, the pivoted arm is raised, creating a small loop. The loop scanner detects any variations in the height or shape of the loop, and it sends a signal to the speed regulator in the PLC. Based on this feedback, the speed of the finishing mill is adjusted to maintain a relatively constant loop height.

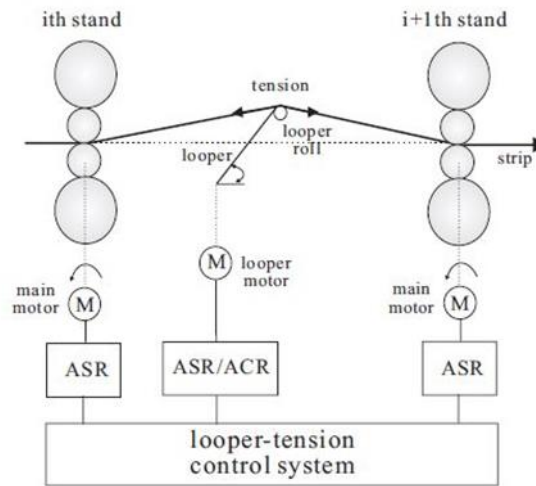


Figure 3.7. Tension and looper control in rolling mills (Source: IEEE xplore)

In hot rolling mills, simultaneous control of looper angle and strip tension can be challenging due to various disturbances from multiple sources. To achieve optimal control performance, it is essential to develop control algorithms that effectively reject these disturbances.

In the finishing end of the rolling mill, the material becomes thinner, and tension can be eliminated by implementing a loop control system. To achieve tension-free rolling, a loop scanner is used to continuously measure the loop height, with the operator setting the desired height and the control algorithm adjusting the mill speed in cascade to maintain a constant loop height. The accuracy of this method depends on the control system and process sensors, which are especially important in high-speed mills where material tracking is critical for loop formation and control sequences.

Traditional infrared loop scanners operate by scanning a narrow measuring area at a  $43^\circ$  angle, enabling it to detect the position of wire, sections, or rods. However, the

presence of dust, steam and loss of sensor view makes the task challenging. The sensor provides an analog output that allows for downstream speed adjustment, centering of hot material, or determining the position of any hot material. In addition, it provides a switching signal to indicate the presence of hot material in the scan area. Figure. 3.8 and Figure 3.9 given below, show the loops formed in hot rolling steel mills as well as the harsh conditions in the mill, respectively.



Figure 3.8. Loop formation in hot rolling mill.



Figure 3.9. Harsh conditions of hot rolling mill.

## CHAPTER 4

### MICROCONTROLLERS AND IMAGE PROCESSING

In this thesis, we propose a novel approach to implementing a loop scanner using image processing and STM32F407G-DISC1 microcontroller. The STM32 microcontroller family is versatile and can be used to build a wide range of embedded systems, from simple battery-powered devices to complex real-time systems. There are many different configurations available with a variety of options for memory, peripherals, performance, and power. Even the simplest devices using STM32 microcontrollers are affordable, making them a good choice for low-volume applications. The peripherals used in the STM32 family are shared across many components and supported by a single firmware library. Therefore, acquiring knowledge on how to program one member of the STM32 family would enable its user to program all of them.

#### 4.1. STM32F407G-DISC1 MICROCONTROLLER

STMicroelectronics has developed a microcontroller called the F407, which belongs to the STM32F4 series. This microcontroller utilizes the Arm Cortex-M4 processor core, providing advanced processing power and digital signal processing capabilities. With a CPU speed of up to 168 MHz and 1MB of Flash memory, the F407 is well-suited for high-performance applications that require sufficient memory space. It has integrated peripherals such as USB, Ethernet, CAN, and multiple serial communication interfaces, making it appropriate for industrial control, automation, robotics, and consumer electronics.

Additionally, the F407 supports low power modes and has a real-time clock for timekeeping purposes. Developers can quickly prototype and develop applications with the help of development tools and software ecosystem like STM32CubeIDE.



Figure 4.1. STM32F407G-DISC1 microcontroller.

#### 4.1.1. Advanced Features of the STM32F407

The STM32 F407 microcontroller is a remarkable device that boasts several advanced features. One of its notable features is the integrated floating-point unit (FPU), which enables it to perform complex mathematical operations, including digital signal processing and control algorithms, with exceptional accuracy and speed. This makes it an excellent choice for applications that require high-performance computing.

The STM32 F407 microcontroller is equipped with advanced analog peripherals, such as a 12-bit analog-to-digital converter (ADC) with up to 24 channels that can sample at a rate of up to 2.4 MSPS. This makes it highly accurate in measuring analog signals. Additionally, it features a 12-bit digital-to-analog converter (DAC) with two channels, providing high precision in generating analog signals. Furthermore, the F407 comes with multiple timers and PWM channels, which enable it to control various types of motors and actuators. It also supports several communication protocols, such as SPI, I2C, USART, and CAN, which simplifies communication with other devices and sensors.

### 4.1.2. STM32 Peripherals

STM32CubeMX is a graphical tool that supports the STM32 F407 microcontroller, making it easy to configure and initialize its peripherals. This tool generates code in multiple programming languages, including C, C++, and Python, which significantly reduces the time and effort required for development.

Moreover, the STM32 F407 microcontroller is compatible with various third-party development tools, including Keil  $\mu$ Vision, IAR Embedded Workbench, and Eclipse. This compatibility enables developers to select their preferred development environment and tools for creating applications on the STM32 F407 platform. In this thesis, CSharp and STM32 microcontroller will be used to control the image capture, processing, and communication with the other components of the system.

## 4.2. IMAGE PROCESSING BASED LOOP SCANNING

### 4.2.1. Advantages

The use of image processing techniques and STM32 microcontrollers offers several advantages over traditional loop scanner systems. Some of the advantages are as follows:

- **Firstly**, cameras are generally less expensive and more reliable than sensors, reducing the overall cost of the system.
- **Secondly**, image processing algorithms can be customized and optimized for specific applications, providing a more accurate and precise way to detect the strip's position and shape.
- **Thirdly**, the use of microcontrollers allows for real-time monitoring and control of the system, enabling operators to quickly identify and respond to any deviations from the desired strip position and shape.

#### 4.2.2. Disadvantages

While the use of image processing techniques and microcontroller technology offers several advantages for loop scanner systems in rolling mills, there are also some potential disadvantages to consider. These include:

- **Complexity:** Image processing algorithms and microcontroller systems can be complex and require specialized expertise to develop and maintain. This could increase the cost and difficulty of implementing and operating a loop scanner system.
- **Maintenance:** Cameras and microcontrollers may require more maintenance than traditional sensors, and failures in these components could lead to downtime and loss of productivity.
- **Environmental factors:** Cameras may be affected by factors such as lighting and dust, which could impact their accuracy and reliability. In addition, microcontrollers may be vulnerable to electromagnetic interference, which could lead to system malfunctions.
- **Integration with existing systems:** Integrating a camera-based loop scanner system with existing control systems and software could be challenging, and could require modifications to the existing infrastructure.

Overall, while there are potential disadvantages of using image processing and microcontroller technology for loop scanning systems in rolling mills, these can often be mitigated through careful planning, implementation, and maintenance. The benefits of improved accuracy, reliability, and efficiency may outweigh the potential drawbacks, making this approach a promising option for the steel industry.

## **CHAPTER 5**

### **EXPERIMENTAL SETUP**

A prototype camera-based loop scanner was designed according to the harsh conditions of the steel rolling mill. The images were taken using ESP32 cam inside the enclosure. The communication of the camera with CSharp and then STM32 microcontroller was conducted via Wifi Module integrated on ESP32 cam.

The experimental setup was prepared in such a way to reflect the genuine case scenarios. Images taken using the loop scanner were processed on CSharp and the generated analog signals on STM32 microcontroller were sent to PLC – SCADA for monitoring. The values were displayed on the SCADA screen and were recorded accordingly. In this chapter, the hardware and software design stages of the loop scanner as well as the prototype designed for testing the loop scanner have been explained in detail.

#### **5.1. LOOP SCANNER DESIGN**

The enclosure shown in Figure 5.1 has been used as a protection for ESP32 cam and is made up of aluminium making it easy to cool down. The enclosure has two small apertures which are used as inlet and outlet for water or air. In our thesis, we used the apertures as inlet and outlet for water to flow all around enclosure for the cooling purposes.



Figure 5.1. Loop scanner design.

Apart from apertures, there is an ON – OFF switch for the camera which turns on and turns off the camera when required. The LED installed at the posterior end has been used as an indication for the turned-on camera. There is a reset button which resets the ESP32 cam in case the images are not seen on our display.

The enclosure consists of an opening at the anterior for the camera to take images as shown in Figure 5.2 below. The camera was fixed inside the enclosure in such a way to take images of the hot rod. There is no cable connection on the Loop Scanner as it operates through Wifi.



Figure 5.2. Camera aperture on loop scanner.

The loop scanner can withstand the harsh conditions of the hot rolling mill. Temperature reaching up to 1200<sup>0</sup>C makes it impossible for the camera to be placed in that environment. The enclosure hinders the heat from reaching the camera. The cooling system continuously circulates the cold water inside the enclosure thus making it safe and appropriate for the camera to operate in such harsh conditions of hot rolling mills.

Figure 5.3 shows the enclosure designed as the protective coating for the camera and Figure 5.4 shows the inner view of the loop scanner.



Figure 5.3. Side view of loop scanner.

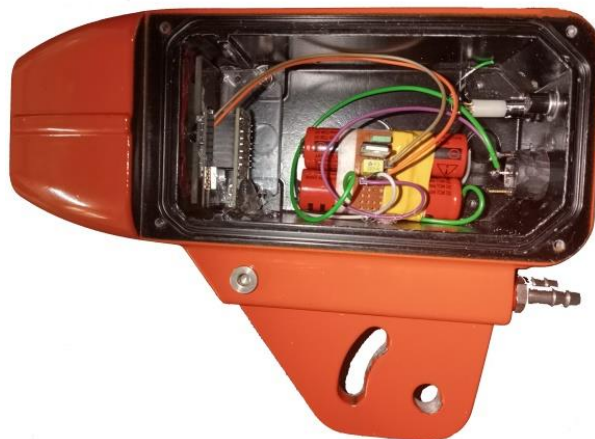


Figure 5.4. Inner view of loop scanner.

## 5.2. SCANNER'S ELECTRICAL COMPONENTS

### 5.2.1. ESP32 CAM

In this thesis, we used an ESP32 CAM which is a small module that combines the ESP32 microcontroller and OV2640 camera module. It is specifically designed for embedded projects such as remote monitoring and video streaming. The module has strong Wi-Fi and Bluetooth capabilities, which make it easy to connect and control the device from IoT devices, smartphones, and tablets. The Wi-fi capability of this device helped us connect it to the IP address and extract the images to csharp programming language where the images were processed.

Despite its small size, ESP32 Cam has a powerful 5MP OV2640 camera sensor that can capture high-quality images with resolutions up to 1600x1200 pixels. We experimented with all the resolution options provided by the device. Keeping the resolution high affected the communication and increased the image processing time. Therefore, we worked on optimal resolution without compromising on the quality of image. ESP32 Cam is given in Figure 5.5 below.



Figure 5.5. ESP32 cam module.

### 5.2.2. Voltage Regulator

There was no cable connection in our design of loop scanner. Therefore, a 7-35V to 5V volatage regulator was designed for the module and a constant 5V was supplied.

L7805C linear regulator and 0.1 $\mu$ F and 0.33 $\mu$ F capacitors were used in the electrical circuit to obtain a constant 5V required for the operation of ESP32 module.

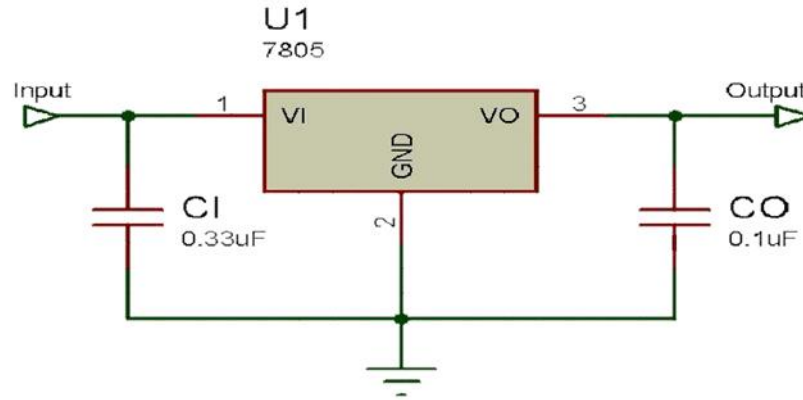


Figure 5.6. Voltage regulator circuit diagram.

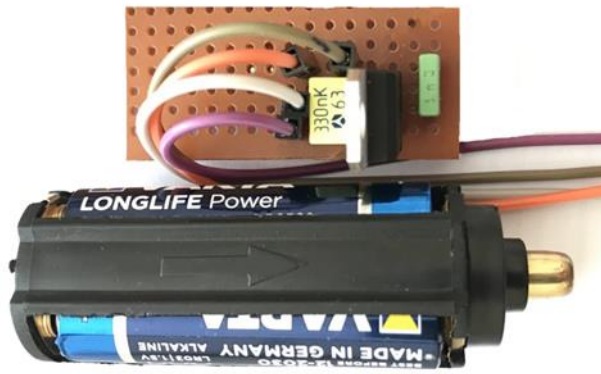


Figure 5.7. Voltage regulator circuit.

### 5.2.3 STM32 Microcontroller

The STM32F407G-DISC development board was used to provide the required analogue signals. This board has an ARM Cortex-M4 processor designed for developing embedded applications and includes various peripherals to aid in this process. Among these peripherals are the UART (Universal Asynchronous Receiver/Transmitter) and DAC (Digital-to-Analog Converter).

The STM32F407G-DISC has several UART interfaces with varying baud rates, which facilitate data exchange between the board and other devices. The DAC is a peripheral that converts digital signals to analog signals. The board features a 12-bit DAC, which can produce analog signals with up to 4096 levels of resolution. This level of precision is ideal for applications such as audio.

#### 5.2.4 STM32 CubeMX

UART and DAC peripherals of STM32 have been used in this thesis to communicate with csharp programming language and provide analogue signals, respectively. STM32CubeMX, a software tool designed by STMicroelectronics to assist developers in configuring STM32 microcontrollers through a user-friendly graphical interface was used to configure the UART and DAC ports. With the help of STM32CubeMX, an initialization code was generated; peripherals and other software components were configured.

A summary of the DAC and UART configuration is depicted in Figure 5.8 and Figure 5.9, whereas clock configuration is given in Figure 5.10 below. This tool simplified our configuration process and aided in starting our project faster.

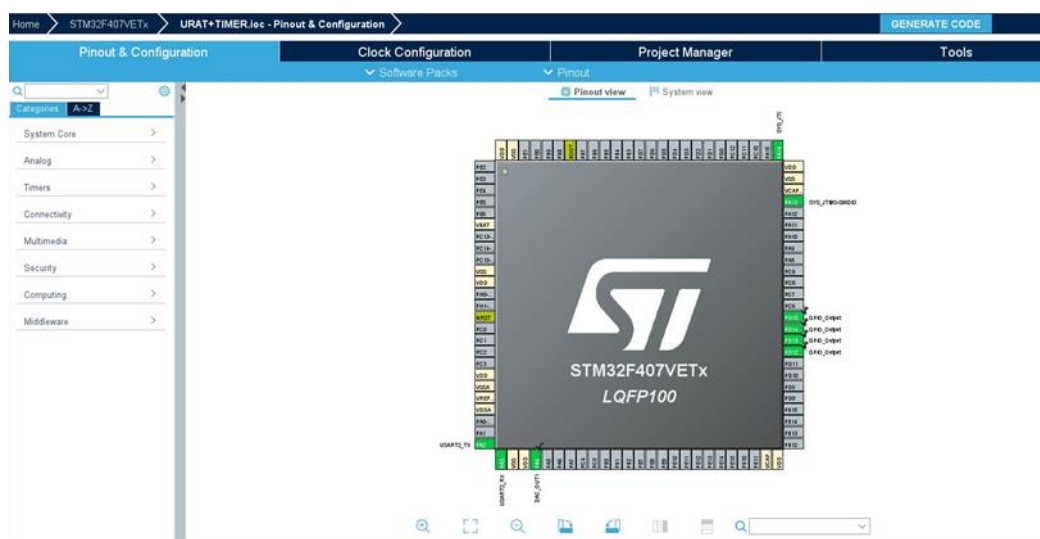


Figure 5.8. STM32 CubeMX configuration.



Figure 5.9. STM32 CubeMX middleware config.

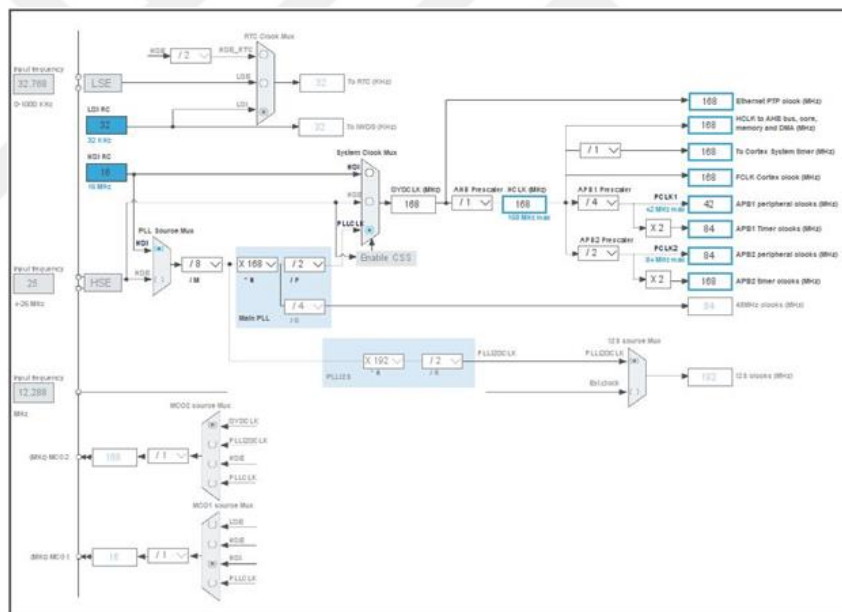


Figure 5.10. STM32 CubeMX clock configuration.

### 5.2.5 S7-1200 PLC

In order to receive the analog signals and display it on SCADA screen, S7-1200 series 1215 DC/DC/DC PLC which is a compact and robust programmable logic controller was used. The PLC used in our thesis has a DC/DC/DC power supply that enables it to operate on a broad range of DC voltages.

The onboard I/O includes 14 digital inputs (DI) that operate at 24V DC, 10 digital outputs (DO) that operate at 24V DC with a current rating of 0.5A, two analog inputs (AI) that can measure voltage in the range of 0-10V DC, and two analog outputs (AO) that can output current in the range of 0-20mA DC.

The power supply requirements for the device are DC 20.4-28.8V DC. The program/data memory of the device is 125 KB in size. Figure 5.11 shows S7 1215C PLC. The S7-1200/1215 DC/DC/DC PLC has a reliable power supply that operates on a broad range of DC voltages, making it well-suited for harsh industrial environments. The device comes equipped with a DC/DC/DC converter that ensures consistent performance despite fluctuations or interruptions in voltage.



Figure 5.11. Simatic S7-1200 PLC.

### 5.2.6 Power Supply

An industrial power supply given in Figure 5.12 was used to provide a maximum output power of 15 watts with a DC adjustable output voltage of 24V to PLC. The power supply is housed in a durable and compact casing that is suitable for use in harsh industrial environments. The power supply has an input voltage range of 100-240VAC.



Figure 5.12. 24V power supply.

### 5.3. MECHANICAL SETUP

The experimental setup consists of a stand made up of steel profile. The stand has a vertically moving part that has a resistance wire attached to it. Single phase supply of 220 volts lights up the resistance. The resistance used in the experimental setup functions as the hot steel which is to be detected in the real system. The constant upwards or downwards movement of the resistance wire is carried out through a moving part on the setup. Figure 5.13, 5.14 and 5.15 given below show experimental setup, resistance wire as well as the designed loop scanner, respectively.



Figure 5.13. Mechanical setup for loop scanning test.



Figure 5.14. Resistance wire used in mechanical setup.



Figure 5.15. Loop scanner detecting resistance wire.

## 5.4. SOFTWARES AND PROGRAMMING

The loop scanning system presented in this thesis undergoes several processes in terms of hardware and software. The block diagram given in Figure 5.16 shows the working principle of the system. Initially, ESP32 cam placed in a closed enclosure captures the images of the loop. This enclosure has been named as loop scanner in this thesis. Then, the loop scanner sends the images captured by camera to PC via Wi-Fi. On PC, images are processed and displayed on the app designed specifically to show the processed image and the original image. Then, depending on the exact location of the loop, an analog signal is generated in STM32 microcontroller. Finally, the analog signal is fed to PLC and displayed on SCADA screen.

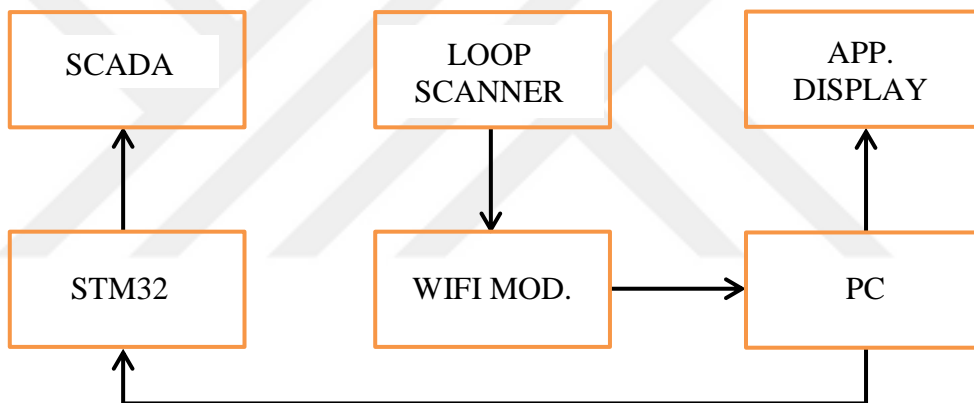


Figure 5.16. Block diagram of loop scanning system.

### 5.4.1 ESP32 CAM Programming

The code was written in Arduino language in which an ESP32-CAM module was connected over Wi-Fi to capture photos. The camera was first set as as "AI\_THINKER" and the required pin definitions were imported from "camera\_pins.h".

```
#include "esp_camera.h"  
#include <WiFi.h>  
#define CAMERA_MODEL_AI_THINKER
```

```
#include "camera_pins.h"
```

The code was then defined for the Wi-Fi credentials asking for ssid and password of the network and executed the "startCameraServer()" function thus setting up a web server to stream the video and provide the necessary visuals.

```
const char* ssid = "*****";  
const char* password = "*****";  
void startCameraServer();
```

In the "setup()" function, the camera was initialized and configured by assigning values to various parameters such as LEDC channel and timer and pin assignments for signals like data, clock and sync. Frame size, JPEG quality, and framebuffer count were set accordingly depending on the availability of PSRAM.

```
void setup() {  
  Serial.begin(115200);  
  Serial.setDebugOutput(true);  
  Serial.println(); ...
```

The function used in the code was altered to apply specific image adjustments for appropriate visuals. A 10-second delay was added between loops. The ESP32 cam was connected to the Wi-Fi network eventually and we were able to start the camera server.

#### **5.4.2 C# (C Sharp) Programming**

Each pixel in a color image is defined by its (R, G, B) coordinates, which together determine the color presented by the pixel. In an 8-bit color bitmap, the range of each color component is [0, 255], resulting in  $255 \times 255 \times 255$  possible color combinations [47]. Processing color images directly involves large amounts of calculations and thus efficiency issues [48]. Therefore, C# Programming language

was used to perform the image processing task. The images captured by the ESP32 cam were transferred to C# software via provided IP address. The C# application was designed to interface with an external device through a serial port to control its behavior based on the output of a loop scanner.

In the programme, the loop scanner captures an image of a particular area and sends it to the application through an HTTP request. The application then performs image processing to identify a particular feature in the image and extract a value from it. This value is used in STM32 microcontroller to output analog signal which in turn controls the looper system via PLC.

The designed application has a GUI that allows the user to enter the IP address of the loop scanner, as well as some other settings such as the range of values to extract from the image and the serial port to use. The code is triggered when the user clicks the "START" button, which is associated with a timer that is set to run at a specified interval. When the timer is started, it calls the "timer1\_Tick", which processes an image displayed in the "pictureBox2".

```
private void timer1_Tick(object sender, EventArgs)
```

```
{
```

```
    pictureBox2.ImageLocation = "http://" + textBox1.Text + "/capture";
```

The code checks if an image is currently displayed in the "pictureBox2". If so, it creates a new "Bitmap" object based on the image and retrieves its width and height.

```
if (pictureBox2.Image != null)
```

```
{
```

```
    Color ReadColor, ConvertedColor;
```

```
    //int R = 0, G = 0, B = 0;
```

```
    int Red;
```

```
    Bitmap InitImage, FinalImage;
```

```
    InitImage = new Bitmap(pictureBox2.Image);
```

```
    int ImageWidth = InitImage.Width;
```

```
    int ImageHeight = InitImage.Height;
```

```
FinalImage = new Bitmap(ImageWidth, ImageHeight);
```

The code then retrieves two integer values from "trackBar1" and "trackBar2", which are used to define a range of values to be mapped to a new grayscale value. If the two values are the same, the code increments the first value by one to avoid a divide-by-zero error.

```
int X1 = trackBar1.Value;  
    int X2 = Convert.ToInt16(trackBar2.Value);  
    if (X1 == X2)  
    {  
        X1++;  
    }
```

The code then creates two integer values, "A" and "B", which represent the minimum and maximum grayscale values.

```
textBox2.Text = X1.ToString();  
    textBox3.Text = X2.ToString();  
    int A = 0; //Convert.ToInt16(textBox3.Text);  
    int B = 255; //Convert.ToInt16(textBox4.Text);
```

The code then runs loops through each pixel in the input image, retrieves its grayscale value, and uses linear interpolation to map the value to a new grayscale value between "A" and "B". The new value is then assigned to a corresponding pixel in the output image.

```
for (int x = 0; x < ImageWidth; x++)  
    {  
        for (int y = 0; y < ImageHeight; y++)  
        {  
            ReadImage = InitImage.GetPixel(x, y);  
            Red = ReadColor.R;
```

```

    int Grey = Red;
    int X = Grey;
    int C = (((X - X1) * (B - A)) / (X2 - X1)) + A;
    if (C > 255) C = 255;
    if (C < 0) C = 0;
    ConvertedColor = Color.FromArgb(C, C, C);
    FinalImage.SetPixel(x, y, ConvertedColor);
}
}

```

The processed image is then displayed in the "pictureBox1" control. The code then retrieves the grayscale value of the center pixel in the output image, and uses it to calculate a value to send over a serial port connection.

```

pictureBox1.Image = null;
pictureBox1.Image = FinalImage;
Bitmap g = new Bitmap(pictureBox1.Image);
for (int y = 0; y < g.Height; y++)
{
    ReadColor = g.GetPixel(g.Width / 2, y);
    if (ReadColor.B < 70 && ReadColor.R < 70 && ReadColor.G < 70)
    {
        label1.Text = y.ToString();
        break;
    }
}
for (int y = g.Height; y >= 0; y--)
{
    try
    {
        ReadColor = g.GetPixel(g.Width / 2, y);
        if (ReadColor.B < 70 && ReadColor.R < 70 && ReadColor.G < 70)
        {

```

```

        label2.Text = y.ToString();
        break;
    }
}
catch { }
}
float ghg = 255f / g.Height;
label3.Text = (255-(Convert.ToInt32(label1.Text)*(ghg))).ToString() ;
int gh = (int)(255 - (Convert.ToInt32(label1.Text) * (ghg)));
if (gh > 255) gh = 255;
if (gh < 0) gh = 0;
byte[] datasend= { (byte)gh };
serialPort1.Write(datasend, 0, 1);
}

```

The flow chart given in Figure 5.17 below shows the general steps implemented in the image processing. The afore-mentioned codes perform the functions provided by the flowchart step by step.

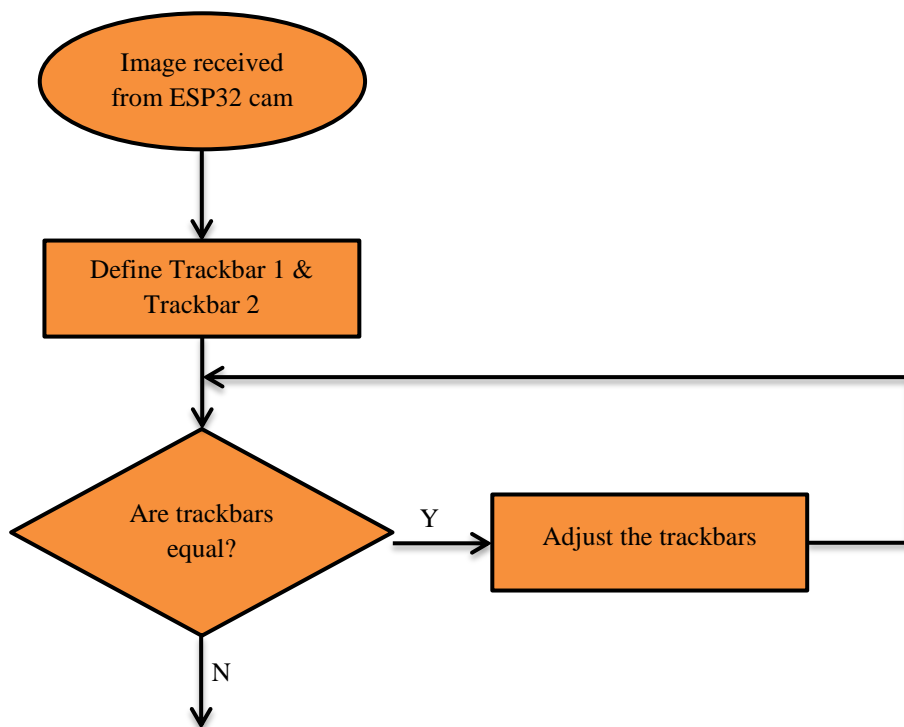


Figure 5.17. Image processing flow chart. (to be continued)

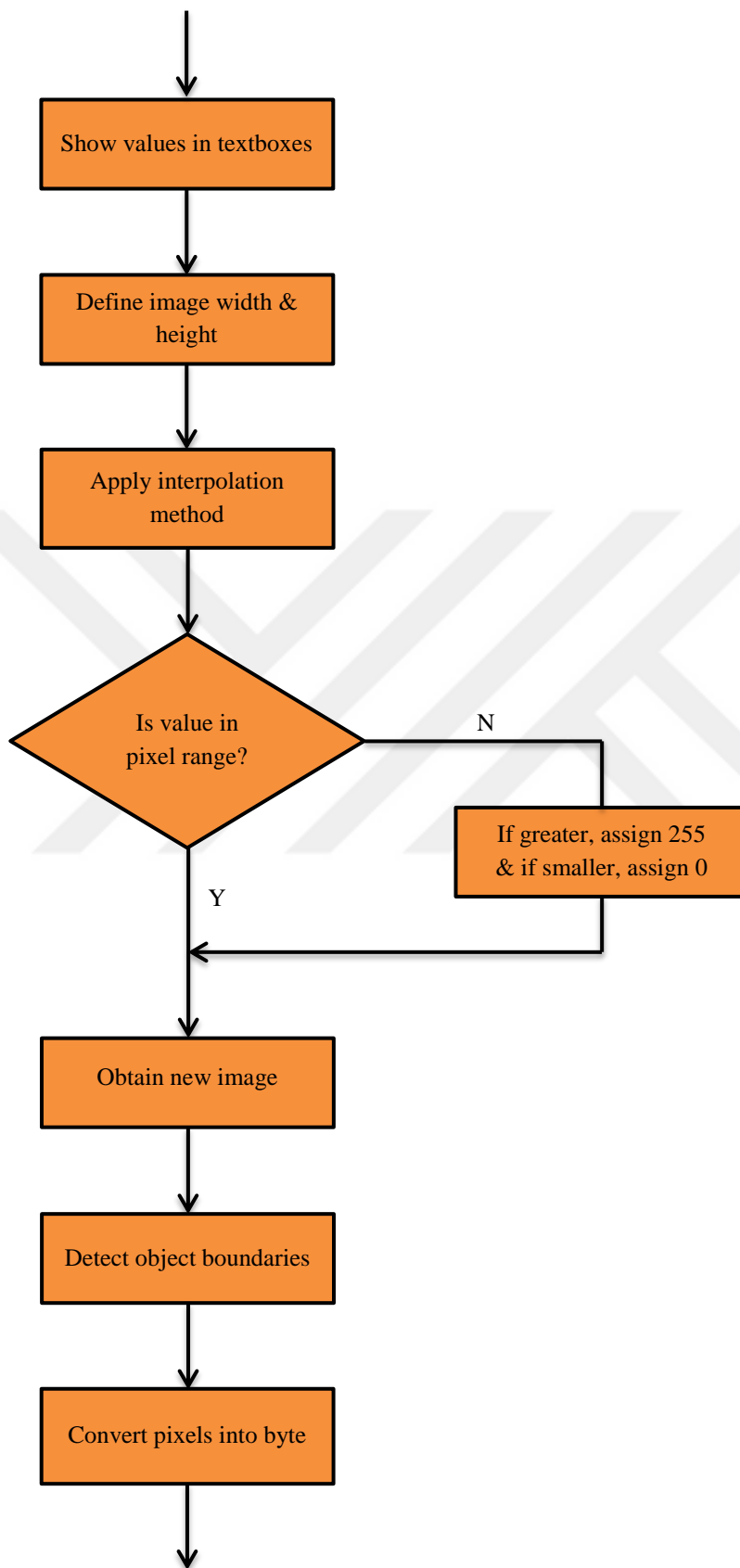


Figure 5.17. Image processing flow chart. (to be continued)

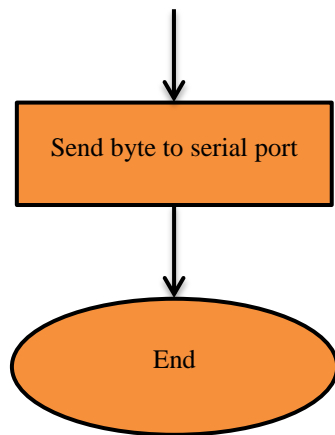


Figure 5.17. Image processing flow chart.

The application thus designed uses the .NET framework's System.Windows.Forms namespace to create the GUI and handle user input. It also uses the System.IO.Ports namespace to communicate with the external device through the serial port.

The image processing algorithm used in the application was effective. The color image was first converted to grayscale, then interpolation method was applied to map a range of grayscale values to a range of output values. This was done using a linear transformation that mapped a range of input values to a range of output values specified by the user.

The resulting grayscale image was then scanned vertically to identify the top and bottom positions of our steel prototype, which was assumed to be a straight rod in the image. The distance between the two positions was used to calculate a value that was sent to STM32 microcontroller through the serial port.

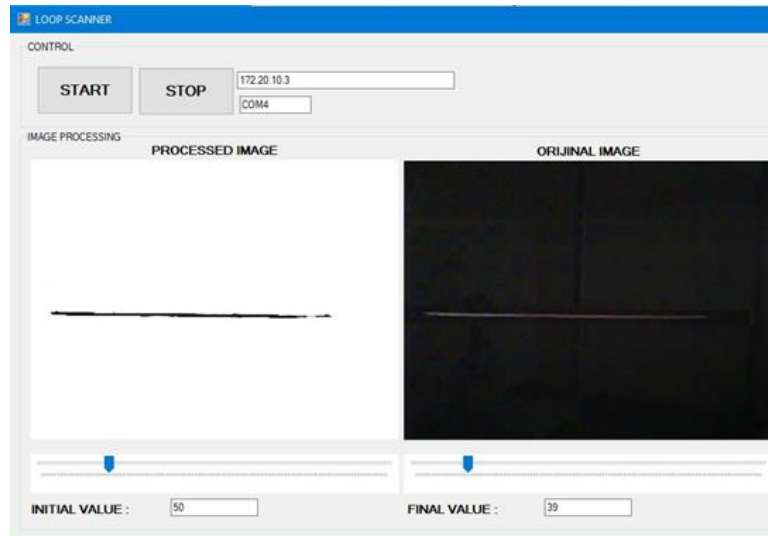


Figure 5.18. Loop scanner application display I.

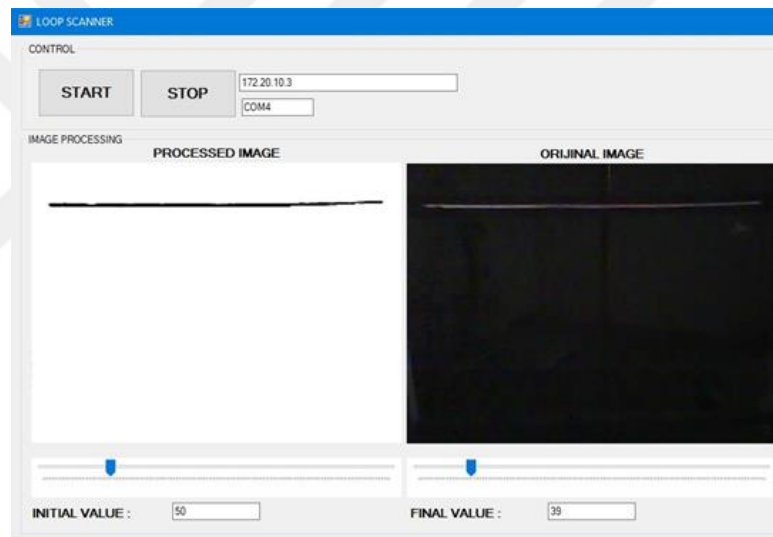


Figure 5.19. Loop scanner application display II.

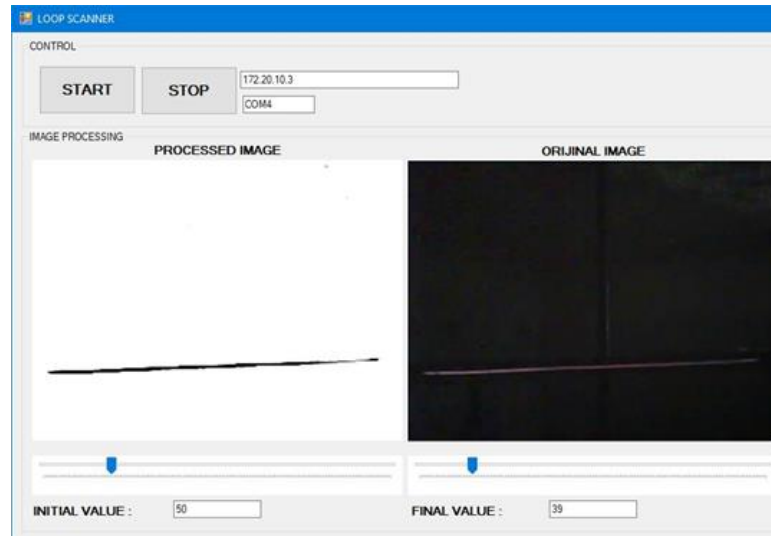


Figure 5.20. Loop scanner application display II.

Overall, this application uses image processing algorithm to be used to provide the processed data based on visual feedback from a loop scanner to microcontroller.

### 5.4.3 STM32 Cube IDE Programming

STM32 Cube IDE was used as Integrated Development Environment (IDE) to programme and debug STM32 microcontroller. We used the program to initialize the necessary modules such as GPIO, UART, DAC, and TIM1. The necessary header files were included at the top of the file. Global variables were defined, including arrays to hold data from the UART and DAC channels. Function prototypes for functions used in the program were also declared.

The main function was initiated with HAL (Hardware Abstraction Layer) initialization, followed by initializing the system clock, GPIO (General-Purpose Input/Output), TIM (Timer), UART, and DAC peripherals.

```
void SystemClock_Config(void);
static void MX_GPIO_Init(void);
static void MX_TIM1_Init(void);
static void MX_USART2_UART_Init(void);
static void MX_DAC_Init(void);
```

The `HAL_TIM_PeriodElapsedCallback()` function has been used as a callback function for the timer interrupt. Whenever the timer period is elapsed, it toggles the state of the pin `GPIOD_Pin_12`. In the main loop, the program waits for any data to be received on the UART, and when data is received, it writes the data to the DAC output pin. The data received is first converted to an integer and then multiplied by 4096 and divided by 255, which scales the data to fit into the range of the DAC output.

```
void HAL_TIM_PeriodElapsedCallback(TIM_HandleTypeDef *htim)
{
HAL_GPIO_TogglePin(GPIOD,GPIO_PIN_12);
}
int main(void)
{
    HAL_Init();
    SystemClock_Config();
    MX_GPIO_Init();
    MX_TIM1_Init();
    MX_USART2_UART_Init();
    MX_DAC_Init();
    HAL_DAC_Start(&hdac, DAC_CHANNEL_1);
    while (1)
    {
HAL_UART_Receive(&huart2,DATA,1,1000);
        DAC1->DHR12R1=(int)DATA[0]*4096/255;
    } ...
}
```

The `SystemClock_Config()` function used was responsible for setting up the system clock, and `MX_DAC_Init()` function was used to initialize the digital-to-analog converter. The `MX_TIM1_Init()` function initialized the timer 1 module in our code. The `MX_USART2_UART_Init()` function set up the UART communication protocol with the baud rate of 115200.

Overall, the code was used to set up the STM32 microcontroller to receive data on the UART and convert it into an analog signal on the DAC output pin. The timer module was also used to toggle the LED to indicate that the program was running.

#### 5.4.4 TIA Portal Programming

After having a DAC output from STM32 microcontroller, PLC S7-1200 1215 DC/DC/DC was used in order to receive 0-3.3V signal and show the data on PC screen after processing it and getting the required output. TIA Portal V15 was used to program the system. Simatic Step 7 TIA Portal V15 interface was used to program the PLC and SCADA software. The programming language used in the programming was ladder programming. Instead of a physical HMI panel, the operator panel was simulated on a computer (PC) screen through SIMATIC HMI Application/WinCC RT Advanced. Figure 5.21 displays the "Device&Networks" view, Figure 5.22 shows the "Portal View" of the TIA Portal project that was created, while Figure 5.23 show the device configuration view.

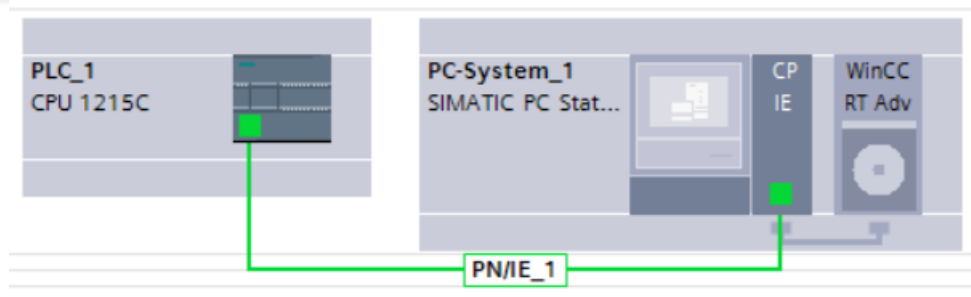


Figure 5.21. Device&Networks view.

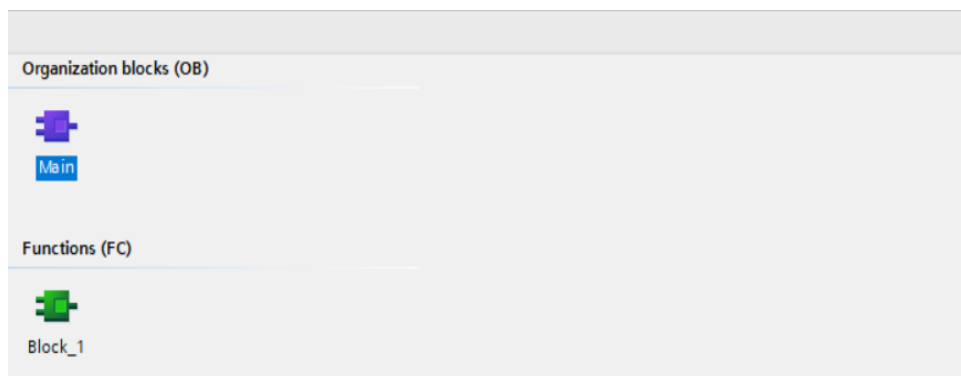


Figure 5.22. Portal view.

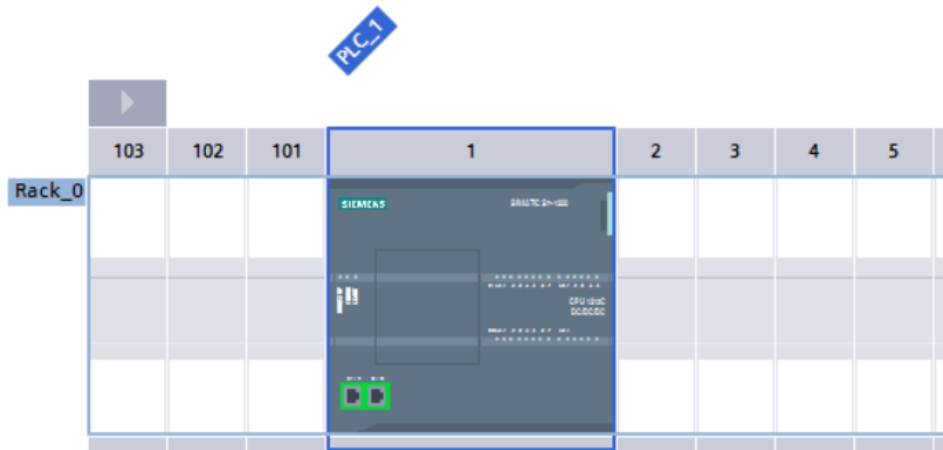


Figure 5.23. Device config. view.

There were a total of 2 analog inputs on PLC S7-1200 1215 DC/DC/DC. Only 1 analog input (AI) was used to receive the 0-3.3V signal from the DAC of STM32. The aim was to design a SCADA screen for the system where the main control of the looper system is carried out. However, the control of the looper system was out of the scope of this thesis. Therefore, only the signal received from STM32 was processed and depicted on SCADA screen.

As the input of analog port for PLC S7-1200 1215 DC/DC/DC is 0-10V, the 0-3.3V signal received from STM32 was normalized and scaled to 0-10V using NORMX and SCALEX functions. A function block was created where OUT\_RANGE function, NORMX and SCALEX functions were used accordingly as shown in Figure 5.24, Figure 5.25 and Figure 5.25, respectively.

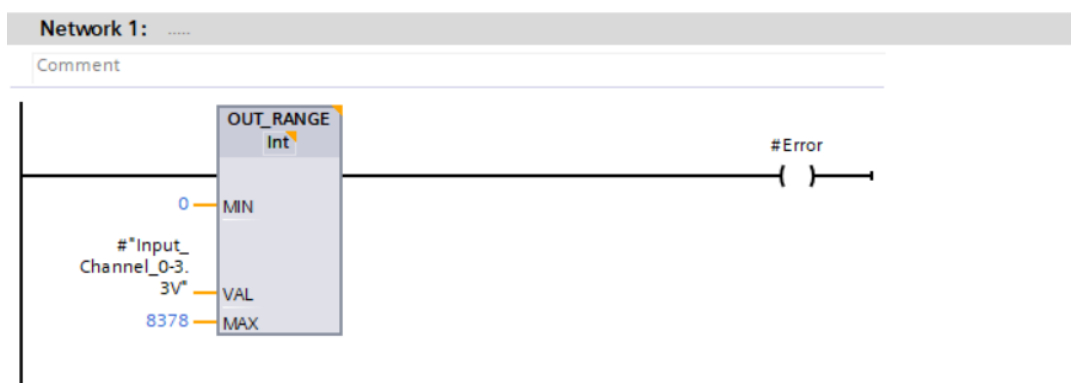


Figure 5.24. Ladder diagram of OUT\_RANGE function.

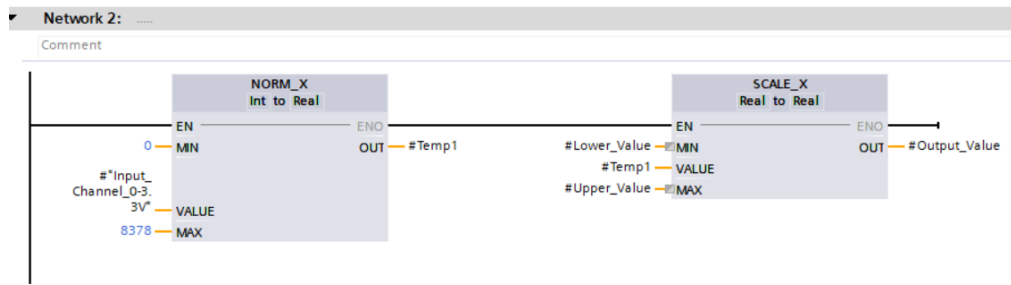


Figure 5.25. Ladder diagram of NORM\_X & SCALE\_X.

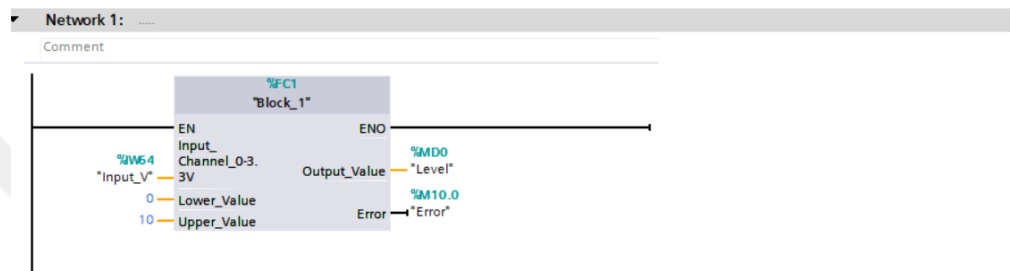


Figure 5.26. Function block.

A function block was created in order to put the values according to calculated values of the project. %IW64 integer word tagged as 'Input\_V' was used as the input channel for 0-3.3V analog input. The value was scaled to 0-10V after being normalized. The output value was shown as memory double word which is a 32-bit integer data type.

The SCADA screen designed for the visualization of loop scanner output was used to monitor real-time values provided after image processing. The screen can further be enhanced to control the looper system according to the feedback values obtained from processed image. The looper control system was not included in this thesis as this would increase the scope of research and would require enormous amount of time.

In the SCADA screen designed for the monitoring purpose of the loop scanner output, 2 graphical bars were used. The first bar shows the analog input signal received from the STM32. The signal ranges from 0 to 8378 obtained by dividing 27648 by 3.3. The maximum value shown on the input side is 8378 which

corresponds to 3.3 volts. On the second bar, the value is scaled between 0-10 and is shown in the box as a final value observed on the SCADA screen.

The value scaled between 0-10 represents the 0-10V of the PLC output which can be used to detect the loop's height when calculated per pixel of the processed image. The value in the box is highlighted using three colors as shown in Figure 5.27, Figure 5.28 and Figure 5.29 below. Three different colors denote the status of the loop, if it is low, medium or high, respectively. The relationship between voltage and cm was found experimentally. At one meter distance, the loop scanner was set to output values of the loop prototype. The experimental findings related to correspondence of voltage to cm showed that every 1 volt fluctuation in the voltage corresponds to a 14.7 cm change in the height of the loop.

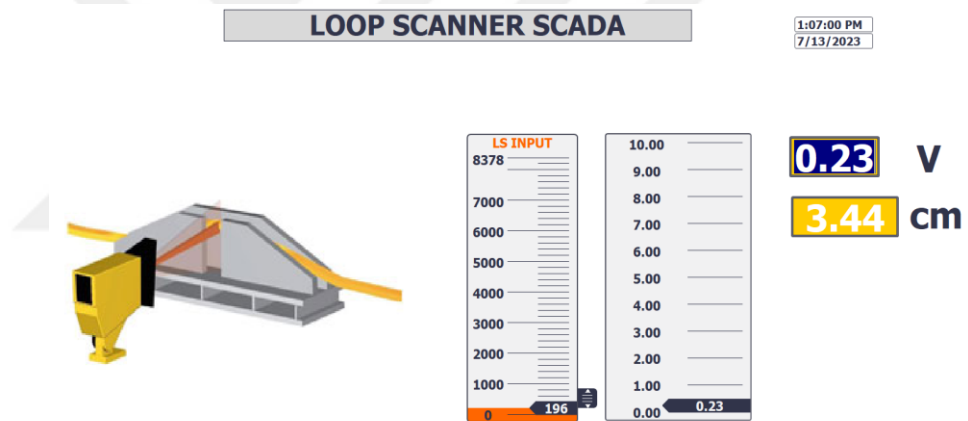


Figure 5.27. SCADA screen 1.

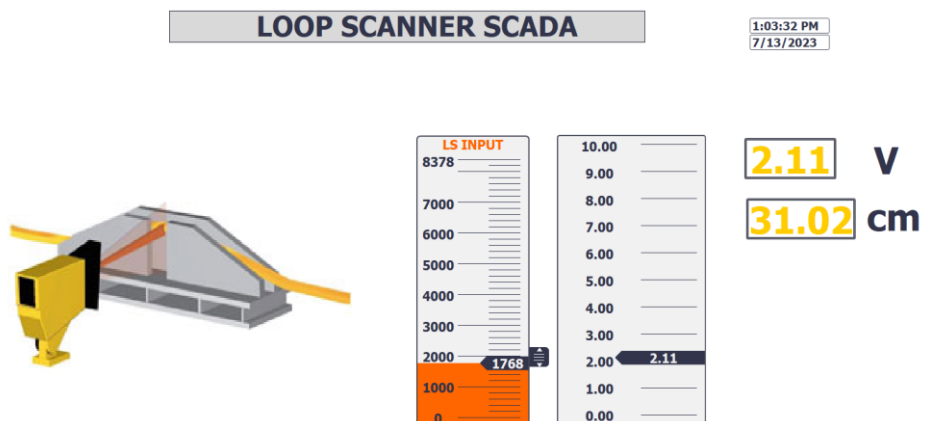


Figure 5.28. SCADA screen 2.

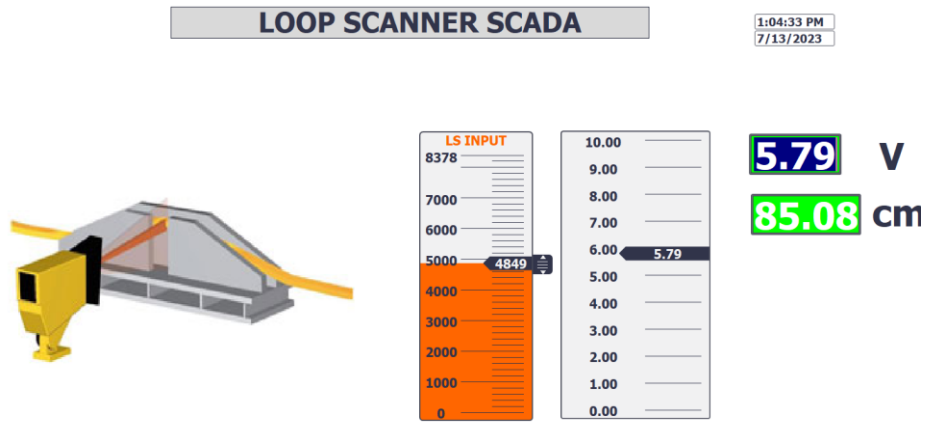


Figure 5.29. SCADA screen 3.

## CHAPTER 6

### CONCLUSIONS AND SUGGESTIONS

#### 6.1. CONCLUSIONS

In this novel research, an ESP32 cam was used to capture the images of the steel rod moving vertically up and down. The captured images were transferred to CSharp via Wi-Fi communication. After processing the images, STM32 microcontroller gave the required DAC output of 0-3.3V. The designed loop scanner was able to scan the loops successfully and satisfactory results were obtained when tested with the experimental setup.

After conducting numerous tests using the designed loop scanner, no flaw was found in the loop detection and processing was performed at a rapid rate. Various results were obtained during the tests and the voltage values were monitored on SCADA screen. The system can be used efficiently in the steel rolling mills as it has all the required specifications.

When compared with the traditional sensor-based loop scanners, the proposed loop scanner is observed to have several advantages. The designed loop scanner is wireless which makes it safer to be used in the rolling mills where the hot steel can come out of the roller way and cut the wires of the loop scanner. Figure 6.1 given below shows the traditional sensors used in the hot rolling mills and their condition after hot steel coming out of the roller way. In addition, the traditional loop scanners are found to be costly. The overall lower cost of the designed loop scanner can be a determining factor in the user preference of the loop scanners. The possibilities of image processing based loop scanner malfunctioning are quite less as compared to the sensors which usually miss the view of the rod and lead to tons of waste in the steel rolling mills.



Figure 6.1. Defected traditional sensors.

## 6.2. SUGGESTIONS

While the proposed system has shown promising results, there is still room for improvement and further exploration. Some potential areas for future work include:

- Enhancing the accuracy and robustness of image processing algorithms by integrating machine learning techniques.
- Employing multiple cameras from different angles to capture a comprehensive view of the strip's position and shape.
- Developing a real-time monitoring and control system that enables operators to promptly identify and address any deviations from the desired strip position and shape.
- Assessing the performance and feasibility of the proposed approach in a real-world rolling mill under actual production conditions.
- Exploring alternative camera types, such as infrared or thermal imaging cameras, to capture strip images in various lighting conditions.

Overall, the proposed method has the potential to revolutionize loop scanner systems in rolling mills, offering a more precise, dependable, and efficient means of controlling strip position and shape. The utilization of CSharp Programming and STM32 microcontrollers for image processing opens up new opportunities for real-time monitoring and control of steel production processes, resulting in enhanced quality and productivity.



## REFERENCES

1. Aldunin, A. Development of method for calculation of structure parameters of hot-rolled steel strip for sheet stamping. *J. Chem. Technol. Metall.* 2017, 52, 737–740.
2. Xu, Z.; Liu, X.; Zhang, K. Mechanical Properties Prediction for Hot Rolled Alloy Steel Using Convolutional Neural Network. *IEEE Access* 2019, 7, 47068–47078.
3. Internet: World Steel Association, “2022 World Steel Statistics” <https://worldsteel.org/steel-topics/statistics/world-steel-in-figures-2022/> (2022).
4. Internet: Online Foreks News, “Turkish Economy News” <https://foreks.com/haber/detay/63d8fa17d6018000015553fb/PICNEWS/tr/turkiye-2022-yilinda-dunya-ham-celik-uretimi-siralamasinda-bir-sira-geriye-dustu> (2023).
5. Internet: Turkey Steel Producers’ Association, “2023 Steel Reports” <https://celik.org.tr/turkiye-celik-ureticileri-dernegi-basin-bulteni-60/> (2023).
6. Dastres and Soori “Advanced Image Processing Systems”, *International Journal of Imaging and Robotics*, Volume 21; Issue No. 1; 2021.
7. Hongnan Liang, Heming Jia, Zhikai Xing, Jun Ma, And Xiaoxu Peng, “Modified Grasshopper Algorithm-Based Multilevel Thresholding for Color Image Segmentation”, *IEEE Access* (2019), Vol-7, PP- 11258–11295.
8. Zhicheng Zhang And Jianqin Yin, “Bee Foraging Algorithm Based Multi-Level Thresholding For Image Segmentation”, *IEEE Access* (2020), Vol-8, PP- 16269–16280.
9. Kostenetskiy, P.; Alkapov, R.; Vetoshkin, N.; Chulkevich, R.; Napolskikh, I.; Poponin, O. Real-time system for automatic cold strip surface defect detection. *FME Trans.* 2019, 47, 765–774.
10. Mazur, I.; Koinov, T. Quality Control system for a hot-rolled metal surface. *Frat. Ed Integrità Strutt.* 2016, 10, 287–296.
11. Internet: “Severstal is Mastering the Production of Video Inspection Systems for Rolled Surfaces”. <https://metallurgprom.org/en/press-releases/4952-severstal-osvaivaet-izgotovlenie-sistem-videoinspekcii-poverhnosti-prokata.html> (2020).

12. Karthikeyan, S.; Pravin, M.C.; Sathyabama, B.; Mareeswari, M. DWT Based LCP Features for the Classification of Steel Surface Defects in SEM Images with KNN Classifier. *Aust. J. Basic Appl. Sci.* 2016, 10.
13. Zaghdoudi, R.; Seridi, H.; Boudiaf, A. Multiple classifier combination for steel surface inspection. *In Proceedings of the 2nd Conference on Informatics and Applied Mathematics*, IAM 2019, Guelma, Algeria, 24–25 April 2019.
14. Samsudin S.S., Arof H., Harun S.W., Wahab A.W.A., Idris M.Y.I. Steel surface defect classification using multi-resolution empirical mode decomposition and LBP. *Meas. Sci. Technol.* 2020;32:015601. doi: 10.1088/1361-6501/abab21.
15. Zhang J., Wang H., Tian Y., Liu K. An accurate fuzzy measure-based detection method for various types of defects on strip steel surfaces. *Comput. Ind.* 2020;122:103231. doi: 10.1016/j.compind.2020.103231.
16. Liu, Y.; Xu, K.; Xu, J. An improved MB-LBP defect recognition approach for the surface of steel plates. *Appl. Sci.* 2019, 9, 4222.
17. Liu L.M., Chu M.X., Gong R.F., Qi X.Y. Unbalanced classification method using least squares support vector machine with sparse strategy for steel surface defects with label noise. *J. Iron. Steel. Res. Int.* 2020;27:1407–1419. doi: 10.1007/s42243-020-00499-6.
18. Li J., Su Z., Geng J., Yin Y. Real-time detection of steel strip surface defects based on improved yolo detection network. *IFAC PapersOnLine.* 2018;51:76–81. doi: 10.1016/j.ifacol.2018.09.412.
19. I. Bello, B. Zoph, Q. Le, A. Vaswani, and J. Shlens. Attention augmented convolutional networks. *In ICCV, 2019.*
20. Han Hu, Jiayuan Gu, Zheng Zhang, Jifeng Dai, and Yichen Wei. Relation networks for object detection. *In CVPR, 2018.*
21. Nicolas Carion, Francisco Massa, Gabriel Synnaeve, Nicolas Usunier, Alexander Kirillov, and Sergey Zagoruyko. End-to-end object detection with transformers. *In ECCV, 2020.*
22. Xiaolong Wang, Ross Girshick, Abhinav Gupta, and Kaiming He. Non-local neural networks. *In CVPR, 2018.*

23. Bichen Wu, Chenfeng Xu, Xiaoliang Dai, Alvin Wan, Peizhao Zhang, Masayoshi Tomizuka, Kurt Keutzer, and Peter Vajda. Visual transformers: Token-based image representation and processing for computer vision. *arxiv*, 2020.
24. Francesco Locatello, Dirk Weissenborn, Thomas Unterthiner, Aravindh Mahendran, Georg Heigold, Jakob Uszkoreit, Alexey Dosovitskiy, and Thomas Kipf. Object-centric learning with slot attention. *arXiv*, 2020.
25. Mark Chen, Alec Radford, Rewon Child, Jeff Wu, and Heewoo Jun. Generative pretraining from pixels. *In ICML, 2020*.
26. Wang L., Xu K., Zhou P. Online detection technique of 3D defects for steel strips based on photometric stereo; *Proceedings of the 2016 Eighth International Conference on Measuring Technology and Mechatronics Automation (ICMTMA)*; Macau, China. 11–12 March 2016; Berlin, Germany: Springer; 2016.
27. Qizhe Xie, Minh-Thang Luong, Eduard Hovy, and Quoc V. Le. Self-training with noisy student improves imagenet classification. *In CVPR, 2020*.
28. Chen Sun, Abhinav Shrivastava, Saurabh Singh, and Abhinav Gupta. Revisiting unreasonable effectiveness of data in deep learning era. *In ICCV, 2017*.
29. Alexander Kolesnikov, Lucas Beyer, Xiaohua Zhai, Joan Puigcerver, Jessica Yung, Sylvain Gelly, and Neil Houlsby. Big transfer (BiT): General visual representation learning. *In ECCV, 2020*.
30. Djolonga, J., Yung, J., Tschannen, M., Romijnders, R., Beyer, L., Kolesnikov, A., Puigcerver, J., Minderer, M., D’Amour, A., Moldovan, D., Gelly, S., Houlsby, N., Zhai, X., & Lucic, M. (2021, June). On Robustness and Transferability of Convolutional Neural Networks. *IEEE/CVF Conference on Computer Vision and Pattern Recognition (CVPR)* 2021.
31. Xue, B., Wu, Z.: Key technologies of steel plate surface defect detection system based on artificial intelligence machine vision. *Wireless Communications and Mobile Computing 2021* (2021).
32. Caleb, P., Steuer, M.: Classification of surface defects on hot rolled steel using adaptive learning methods. In: KES’2000. *Fourth International Conference on Knowledge-Based Intelligent Engineering Systems and Allied Technologies. Proceedings* (Cat. No. 00TH8516). vol. 1, pp. 103-108. IEEE (2000).

33. Zhao, Z., Qi, H., Qi, Y., Zhang, K., Zhai, Y., Zhao, W.: Detection method based on automatic visual shape clustering for pin-missing defect in transmission lines. *IEEE Transactions on Instrumentation and Measurement* **69(9)**, 6080-6091 (2020).
34. Liu, W., Liu, Z., Nunez, A., Han, Z.: Unified deep learning architecture for the detection of all catenary support components. *IEEE Access* **8**, 17049-17059 (2020).
35. Song, L., Li, X., Yang, Y., Zhu, X., Guo, Q., Yang, H.: Detection of micro-defects on metal screw surfaces based on deep convolutional neural networks. *Sensors* **18 (11)**, 3709 (2018).
36. Taheritanjani, S., Schoenfeld, R., Bruegge, B.: Automatic damage detection of fasteners in overhaul processes. *In: 2019 IEEE 15th International Conference on Automation Science and Engineering (CASE)*. pp. 1289-1295. IEEE (2019).
37. Urbano, CF Ordóñez, and J. L. Téllez. "Implementation and calibration of a laser Doppler velocimeter in order to measure liquids velocity." *Rev. Mex. Fis. S* **59.1** (2013): 84-89.
38. Indu, S., Gupta, M., & Bhattacharyya, A. (2011). Vehicle tracking and speed estimation using optical flow method. *Int. J. Engineering Science and Technology*, 3(1), 429-434.
39. Souto, M. L., Fernández, A., & Guerra, L. (2020). Real machine vision use-cases applied to hot rolling mill plants. *Procedia Manufacturing*, **51**, 280–287. <https://doi.org/10.1016/j.promfg.2020.10.040> (2020).
40. Lenard, J. G. (2001, June 30). Friction During Flat Rolling of Metals. *International Journal of Forming Processes*, 4(1–2), 23–41. <https://doi.org/10.3166/ijfp.4.23-41>
41. Internet: Understanding Grain Structure and Direction when Plate Bending, <https://www.barnshaws.com/information/articles/understanding-grain-structure-and-direction-when-plate-bending> (2018).
42. I. S. Choi, J. A. Rossiter, and P. J. Fleming, "Looper and tension control in hot rolling mills: A survey," *Journal of Process Control*, vol. 17, pp. 509–521, 2007.
43. B. Q. Li, K. J. Zhang, J. Fu, and Y. K. Sun, "Diagonal Recurrent Neural Network Decoupling Control on The Looper's Height and Tension System," *in Proceedings of the 6th World Congress on Control and Automation, Dalian, China*, June 21- 23, 2006, pp. 2787–2791.

44. Neto, A. F., Pereira, S. L., Dias, E. M., & Scoton, M. L. R. D. (2021). Looper angle and looper tension control between roll stands in hot strip finishing mills in adaptive, predictive Proportional Integral (PI) and Inverse Linear Quadratic (ILQ) control modes, with activation by means of servo valves and hydraulic cylinders. *International Journal of Advanced Engineering Research and Science*, 8(5), 323–344.
45. SUN, X. and H.-F. SUN. Speed cascade control system for bar and wire rod mills. ABB China Ltd [online]. 2015. Available at: <https://library.e.abb.com/public/4cb4384eb21fc2738525761f004fc27b/1618%20Speed%20Cascade%20VP.pdf>.
46. Hot Metal Detector and Loop Scanners for Rolling Mills and Casters. Pacific International Pvt [online]. 2017. Available at: <http://www.pacificinternational.co.in>.
47. Geddada N , Yeap Y M , Ukil A . Experimental validation of fault identification in VSC based DC grid[J]. *IEEE Trans. Ind. Electr.* 2018;65(6):4799–809.
48. Srinivasan S M , Truong-Huu T , Gurusamy M . Machine learning-based link fault identification and localization in complex networks[J]. *IEEE Internet of Things J.* 2019;6(4):6556–66.



**APPENDIX A.**

**ESP32-CAM CODE**

```

#include "esp_camera.h"

#include <WiFi.h>

#define CAMERA_MODEL_AI_THINKER

#include "camera_pins.h"

const char* ssid = "iPhone";

const char* password = "Kamal1995";

void startCameraServer();

void setup() {
  Serial.begin(115200);
  Serial.setDebugOutput(true);
  Serial.println();

  camera_config_t config;

  config.ledc_channel = LEDC_CHANNEL_0;
  config.ledc_timer = LEDC_TIMER_0;

  config.pin_d0 = Y2_GPIO_NUM;
  config.pin_d1 = Y3_GPIO_NUM;
  config.pin_d2 = Y4_GPIO_NUM;
  config.pin_d3 = Y5_GPIO_NUM;
  config.pin_d4 = Y6_GPIO_NUM;
  config.pin_d5 = Y7_GPIO_NUM;
  config.pin_d6 = Y8_GPIO_NUM;
  config.pin_d7 = Y9_GPIO_NUM;

  config.pin_xclk = XCLK_GPIO_NUM;
  config.pin_pclk = PCLK_GPIO_NUM;
  config.pin_vsync = VSYNC_GPIO_NUM;

```

```

config.pin_href = HREF_GPIO_NUM;
config.pin_sscb_sda = SIOD_GPIO_NUM;
config.pin_sscb_scl = SIOC_GPIO_NUM;
config.pin_pwdn = PWDN_GPIO_NUM;
config.pin_reset = RESET_GPIO_NUM;
config.xclk_freq_hz = 20000000;
config.pixel_format = PIXFORMAT_JPEG;

```

```

if(psramFound()){
    config.frame_size = FRAMESIZE_UXGA;
    config.jpeg_quality = 10;
    config.fb_count = 2;
} else {
    config.frame_size = FRAMESIZE_SVGA;
    config.jpeg_quality = 12;
    config.fb_count = 1;
}

```

```

#if defined(CAMERA_MODEL_ESP_EYE)

```

```

    pinMode(13, INPUT_PULLUP);

```

```

    pinMode(14, INPUT_PULLUP);

```

```

#endif

```

```

esp_err_t err = esp_camera_init(&config);

```

```

if (err != ESP_OK) {

```

```

    Serial.printf("Camera init failed with error 0x%x", err);

```

```

    return;

```

```

}

```

```

sensor_t * s = esp_camera_sensor_get();

```

```

if (s->id.PID == OV3660_PID) {

```

```

s->set_vflip(s, 1); // flip it back

s->set_brightness(s, 1); // up the brightness just a bit

s->set_saturation(s, -2); // lower the saturation

}

s->set_framesize(s, FRAMESIZE_QVGA);

#if defined(CAMERA_MODEL_M5STACK_WIDE) ||
defined(CAMERA_MODEL_M5STACK_ESP32CAM)

s->set_vflip(s, 1);

s->set_hmirror(s, 1);

#endif

WiFi.begin(ssid, password);

while (WiFi.status() != WL_CONNECTED) {

  delay(500);

  Serial.print(".");

}

Serial.println("");

Serial.println("WiFi connected");

startCameraServer();

Serial.print("Camera Ready! Use 'http://");

Serial.print(WiFi.localIP());

Serial.println("' to connect");

}

void loop() {

  delay(10000);

}

```



**APPENDIX B.**

**C# CODE**

```

using System;
using System.Collections.Generic;
using System.ComponentModel;
using System.Data;
using System.Drawing;
using System.Linq;
using System.Text;
using System.Threading.Tasks;
using System.Windows.Forms;
using System.IO.Ports;

namespace loop_scanner1
{
    public partial class Form1 : Form
    {
        public Form1()
        {
            InitializeComponent();
            serialPort1.PortName = textBox4.Text;
        }

        private void Form1_Load(object sender, EventArgs e)
        {
        }

        Image Image = null;

        private void timer1_Tick(object sender, EventArgs e)
        {
            pictureBox2.ImageLocation = "http://" + textBox1.Text + "/capture";
        }
    }
}

```

```

if (pictureBox2.Image != null)
{
    Color ReadColor, ConvertedColor;
    //int R = 0, G = 0, B = 0;
    int Red;
    Bitmap InitImage, FinalImage;
    InitImage = new Bitmap(pictureBox2.Image);
    int ImageWidth = InitImage.Width;
    int ImageHeight = InitImage.Height;
    FinalImage = new Bitmap(ImageWidth, ImageHeight);
    int X1 = trackBar1.Value;
    int X2 = Convert.ToInt16(trackBar2.Value);
    if (X1 == X2)
    {
        X1++;
    }
    textBox2.Text = X1.ToString();
    textBox3.Text = X2.ToString();
    int A = 0; //Convert.ToInt16(textBox3.Text);
    int B = 255; //Convert.ToInt16(textBox4.Text);
    for (int x = 0; x < ImageWidth; x++)
    {
        for (int y = 0; y < ImageHeight; y++)
        {
            ReadColor = InitImage.GetPixel(x, y);
            Red = ReadColor.R;
            int Grey = Red;

            //***** INTERPOLATION METHOD*****

```

```

        int X = Grey;
        int C = (((X - X1) * (B - A)) / (X2 - X1)) + A;
        if (C > 255) C = 255;
        if (C < 0) C = 0;
        ConvertedColor = Color.FromArgb(C, C, C);
        FinalImage.SetPixel(x, y, ConvertedColor);
    }
}
// pictureBox3.Refresh();
pictureBox1.Image = null;
pictureBox1.Image = FinalImage;
Bitmap g = new Bitmap(pictureBox1.Image);
for (int y = 0; y < g.Height; y++)
{
    ReadColor = g.GetPixel(g.Width / 2, y);
    if (ReadColor.B < 70 && ReadColor.R < 70 && ReadColor.G < 70)
    {
        label1.Text = y.ToString();
        break;
    }
}

for (int y = g.Height; y >= 0; y--)
{
    try
    {
        ReadColor = g.GetPixel(g.Width / 2, y);
        if (ReadColor.B < 70 && ReadColor.R < 70 && ReadColor.G < 70)

```

```

        {
            label2.Text = y.ToString();
            break;
        }
    }
    catch { }
}

float ghg = 255f / g.Height;
label3.Text = (255-(Convert.ToInt32(label1.Text)*(ghg))).ToString();
int gh = (int)(255 - (Convert.ToInt32(label1.Text) * (ghg)));
if (gh > 255) gh = 255;
if (gh < 0) gh = 0;
byte[] datasend= { (byte)gh };
serialPort1.Write(datasend, 0, 1);
}
}

private void button1_Click(object sender, EventArgs e)
{
    timer1.Enabled = true;
    serialPort1.Open();
}

private void button2_Click(object sender, EventArgs e)
{
    timer1.Enabled = false;
    serialPort1.Close();
    pictureBox2.Image = null;
    pictureBox1.Image = null;
    label1.Text = "0";
}

```

```

        label2.Text = "0";

        label3.Text = "0";

    }

    private void button3_Click(object sender, EventArgs e)
    {

        SerialPort serialPort12 = new SerialPort("COM6", 115200, Parity.None, 8,
        StopBits.One);

        // Create a new SerialPort object with the appropriate settings

        serialPort12.Open(); // Open the serial port

        byte[] dataToSend = { 0x0a }; // Send data in bytes

        serialPort12.WriteLine("\n");

        serialPort12.Close(); // Close the serial port

    }

    private void button4_Click(object sender, EventArgs e)
    {

        SerialPort serialPort12 = new SerialPort("COM6", 115200, Parity.None, 8,
        StopBits.One);

        serialPort12.Open();

        byte[] dataToSend = { 0x0a };

        serialPort12.Write(dataToSend, 0,1);

        serialPort12.Close();

    }

    private void groupBox2_Enter(object sender, EventArgs e)
    {

    }

}
}

```



**APPENDIX C.**

**STM32 CODE**

```

#include "main.h"

uint8_t DATA[1];
uint8_t ReceivedData[1];
uint8_t data[] = "o \r\n";
DAC_HandleTypeDef hdac;
TIM_HandleTypeDef htim1;
UART_HandleTypeDef huart2;
void SystemClock_Config(void);
static void MX_GPIO_Init(void);
static void MX_TIM1_Init(void);
static void MX_USART2_UART_Init(void);
static void MX_DAC_Init(void);
void HAL_TIM_PeriodElapsedCallback(TIM_HandleTypeDef *htim)
{
    HAL_GPIO_TogglePin(GPIOD,GPIO_PIN_12);
}
int main(void)
{
    HAL_Init();
    SystemClock_Config();
    MX_GPIO_Init();
    MX_TIM1_Init();
    MX_USART2_UART_Init();
    MX_DAC_Init();
    HAL_DAC_Start(&hdac, DAC_CHANNEL_1);
    while (1)
    {

```

```

    }
}
void SystemClock_Config(void)
{
    RCC_OscInitTypeDef RCC_OscInitStruct = {0};
    RCC_ClkInitTypeDef RCC_ClkInitStruct = {0};
    __HAL_RCC_PWR_CLK_ENABLE();

    __HAL_PWR_VOLTAGESCALING_CONFIG(PWR_REGULATOR_VOLTAGE_SCAL
E1);
    RCC_OscInitStruct.OscillatorType = RCC_OSCILLATORTYPE_HSI;
    RCC_OscInitStruct.HSISState = RCC_HSI_ON;
    RCC_OscInitStruct.HSICalibrationValue = RCC_HSICALIBRATION_DEFAULT;
    RCC_OscInitStruct.PLL.PLLState = RCC_PLL_ON;
    RCC_OscInitStruct.PLL.PLLSource = RCC_PLLSOURCE_HSI;
    RCC_OscInitStruct.PLL.PLLM = 8;
    RCC_OscInitStruct.PLL.PLLN = 168;
    RCC_OscInitStruct.PLL.PLLP = RCC_PLLP_DIV2;
    RCC_OscInitStruct.PLL.PLLQ = 4;
    if (HAL_RCC_OscConfig(&RCC_OscInitStruct) != HAL_OK)
    {
        Error_Handler();
    }
    RCC_ClkInitStruct.ClockType =
RCC_CLOCKTYPE_HCLK|RCC_CLOCKTYPE_SYSCLK
|RCC_CLOCKTYPE_PCLK1|RCC_CLOCKTYPE_PCLK2;
    RCC_ClkInitStruct.SYSCLKSource = RCC_SYSCLKSOURCE_PLLCLK;
    RCC_ClkInitStruct.AHBCLKDivider = RCC_SYSCLK_DIV1;
    RCC_ClkInitStruct.APB1CLKDivider = RCC_HCLK_DIV4;

```

```

RCC_ClkInitStruct.APB2CLKDivider = RCC_HCLK_DIV2;

if (HAL_RCC_ClockConfig(&RCC_ClkInitStruct, FLASH_LATENCY_5) != HAL_OK)
{
    Error_Handler();
}
}

static void MX_DAC_Init(void)
{
    DAC_ChannelConfTypeDef sConfig = {0};

    hdac.Instance = DAC;

    if (HAL_DAC_Init(&hdac) != HAL_OK)
    {
        Error_Handler();
    }

    sConfig.DAC_Trigger = DAC_TRIGGER_NONE;

    sConfig.DAC_OutputBuffer = DAC_OUTPUTBUFFER_ENABLE;

    if (HAL_DAC_ConfigChannel(&hdac, &sConfig, DAC_CHANNEL_1) != HAL_OK)
    {
        Error_Handler();
    }

}

static void MX_TIM1_Init(void)
{
    TIM_ClockConfigTypeDef sClockSourceConfig = {0};

    TIM_MasterConfigTypeDef sMasterConfig = {0};

    htim1.Instance = TIM1;

    htim1.Init.Prescaler = 0;

```

```

htim1.Init.CounterMode = TIM_COUNTERMODE_UP;

htim1.Init.Period = 65535;

htim1.Init.ClockDivision = TIM_CLOCKDIVISION_DIV1;

htim1.Init.RepetitionCounter = 0;

htim1.Init.AutoReloadPreload = TIM_AUTORELOAD_PRELOAD_DISABLE;

if (HAL_TIM_Base_Init(&htim1) != HAL_OK)
{
    Error_Handler();
}

sClockSourceConfig.ClockSource = TIM_CLOCKSOURCE_INTERNAL;

if (HAL_TIM_ConfigClockSource(&htim1, &sClockSourceConfig) != HAL_OK)
{
    Error_Handler();
}

sMasterConfig.MasterOutputTrigger = TIM_TRGO_RESET;

sMasterConfig.MasterSlaveMode = TIM_MASTERSLAVEMODE_DISABLE;

if (HAL_TIMEx_MasterConfigSynchronization(&htim1, &sMasterConfig) != HAL_OK)
{
    Error_Handler();
}
}

static void MX_USART2_UART_Init(void)
{
    huart2.Instance = USART2;

    huart2.Init.BaudRate = 115200;

    huart2.Init.WordLength = UART_WORDLENGTH_8B;

    huart2.Init.StopBits = UART_STOPBITS_1;

    huart2.Init.Parity = UART_PARITY_NONE;

```

```

huart2.Init.Mode = UART_MODE_TX_RX;

huart2.Init.HwFlowCtl = UART_HWCONTROL_NONE;

huart2.Init.OverSampling = UART_OVERSAMPLING_16;

if (HAL_UART_Init(&huart2) != HAL_OK)

{

    Error_Handler();

}

}

static void MX_GPIO_Init(void)

{

    GPIO_InitTypeDef GPIO_InitStructure = {0};

    __HAL_RCC_GPIOA_CLK_ENABLE();

    __HAL_RCC_GPIOD_CLK_ENABLE();

    HAL_GPIO_WritePin(GPIOD,
GPIO_PIN_12|GPIO_PIN_13|GPIO_PIN_14|GPIO_PIN_15, GPIO_PIN_RESET);

    GPIO_InitStructure.Pin = GPIO_PIN_12|GPIO_PIN_13|GPIO_PIN_14|GPIO_PIN_15;

    GPIO_InitStructure.Mode = GPIO_MODE_OUTPUT_PP;

    GPIO_InitStructure.Pull = GPIO_NOPULL;

    GPIO_InitStructure.Speed = GPIO_SPEED_FREQ_LOW;

    HAL_GPIO_Init(GPIOD, &GPIO_InitStructure);

}

void Error_Handler(void)

{

    __disable_irq();

    while (1)

    {

    }

}

```

```
#ifdef USE_FULL_ASSERT
void assert_failed(uint8_t *file, uint32_t line)
{
}
#endif
```



## **BIOGRAPHY**

Kamal Uddin AQA earned his bachelor's degree in electrical and electronics engineering from Karabuk University, in 2020. He worked in an electrical automation company between 2020 and 2023. While working, he pursued his graduate studies at Karabuk University.

